

EVOLUTION OF GROUP GALAXIES FROM THE FIRST RED-SEQUENCE CLUSTER SURVEY

I.H. LI^{1,2}, H.K.C. YEE², B.C. HSIEH³, AND M. GLADDERS^{4,5}

Draft version May 31, 2018

ABSTRACT

We study the evolution of the red galaxy fraction (f_{red}) in 905 galaxy groups with $0.15 \leq z < 0.52$. The galaxy groups are identified by the ‘probability Friends-of-Friends’ algorithm from the first Red-Sequence Cluster Survey (RCS1) photometric-redshift sample. There is a high degree of uniformity in the properties of the red-sequence of the group galaxies, indicating that the luminous red-sequence galaxies in the groups are already in place by $z \sim 0.5$ and that they have a formation epoch of $z \gtrsim 2$. In general, groups at lower redshifts exhibit larger f_{red} than those at higher redshifts, showing a group Butcher-Oemler effect. We investigate the evolution of f_{red} by examining its dependence on four parameters, which can be classified as one intrinsic and three environmental: galaxy stellar mass (M_*), total group stellar mass ($M_{*,grp}$, a proxy for group halo mass), normalized group-centric radius (r_{grp}), and local galaxy density (Σ_5). We find that M_* is the dominant parameter such that there is a strong correlation between f_{red} and galaxy stellar mass. Furthermore, the dependence of f_{red} on the environmental parameters is also a strong function of M_* . Massive galaxies ($M_* \gtrsim 10^{11} M_\odot$) show little dependence of f_{red} on r_{grp} , $M_{*,grp}$, and Σ_5 over the redshift range. The dependence of f_{red} on these parameters is primarily seen for galaxies with lower masses, especially for $M_* \lesssim 10^{10.6} M_\odot$. We observe an apparent ‘group down-sizing’ effect, in that galaxies in lower-mass halos, after controlling for galaxy stellar mass, have lower f_{red} . We find a dependence of f_{red} on both r_{grp} and Σ_5 after the other parameters are controlled. At a fixed r_{grp} , there is a significant dependence of f_{red} on Σ_5 , while r_{grp} gradients of f_{red} are seen for galaxies in similar Σ_5 regions. This indicates that galaxy group environment has a residual effect over that of local galaxy density (or vice versa), and both parameters need to be considered. This result suggests that processes identified with local galaxy density, such as galaxy harassment and mergers, and those associated with accretion into a larger group halo, such as ram pressure and strangulation, are both partaking in driving galaxies to their final red quiescent state. We discuss these results in the context of the ‘nature vs nurture’ scenario of galaxy evolution.

Subject headings: galaxies: evolution – galaxies: photometry – galaxies: cluster:general

1. INTRODUCTION

Galaxies evolve with time. Generally speaking, the star formation rate within galaxies decreases as galaxies age, and hence galaxy colors transit from blue to red, and their spiral arms become less and less dominant. It has been known since the 1970’s that red galaxies tend to populate galaxy clusters and blue galaxies are common in the field (Oemler 1974). The fraction of red galaxies decreases from cluster center to the field. Measuring galaxy morphologies in 55 clusters in the nearby Universe, Dressler (1980) found that galaxy population fractions have a stronger dependence on local galaxy density than on cluster-centric radius. This work formulated the well-known ‘morphology-density’ relation, and is generally investigated as the ‘color-density’ relation later on

in the literature (e.g., Kodama et al. 2001; Cooper et al. 2006; Quadri et al. 2007; Cassata et al. 2007; Cooper et al. 2007). This result is interpreted as a decrease in the star formation rate as local galaxy density increases. A ‘critical density’ was suggested to characterize the local galaxy density effect (e.g., Lewis et al. 2002; Gómez et al. 2003; Tanaka et al. 2004) with the concept that star formation rate and galaxy color exhibit abrupt changes when the galaxy density crosses the critical density. Regardless of whether this critical density exists or what its true meaning is, the density where both star formation rates and galaxy colors change rapidly may indicate an environmental transition between galaxy groups and the field (e.g., Kodama et al. 2001; Goto et al. 2003; Balogh et al. 2004; Li et al. 2009, hereafter L09).

Galaxy groups are small galaxy aggregations bound by gravity. Some groups contain a few galaxies while others may have several dozens. This gives galaxy groups a fundamental role in building up large-scale structures, as more and more galaxies are accreted into groups over time and groups merge together. In the local Universe the majority of galaxies are found in galaxy groups (e.g., Geller & Huchra 1983; Fukugita et al. 1998; Eke et al. 2004). Because of their sufficiently high galaxy density and low velocity dispersion, galaxy groups are a favored environment for interactions and mergers, causing most of the galaxy transformations in morphology, star formation rates, and colors (e.g., Ghigna et al. 1998; Mulchaey

Electronic address: tli@astro.swin.edu.au

Electronic address: hyee@astro.utoronto.ca

Electronic address: bchsieh@asiaa.sinica.edu.tw

Electronic address: gladders@oddjob.uchicago.edu

¹ Centre for Astrophysics & Supercomputing, Swinburne University of Technology, PO Box 218, Hawthorn, Victoria 3122, Australia

² 50 St. George Street, Department of Astronomy & Astrophysics, University of Toronto, Toronto, ON, Canada, M5S 3H4

³ Institute of Astronomy and Astrophysics, Academia Sinica, PO Box 23-141, Taipei 106, R.O.C. Taiwan

⁴ Department of Astronomy and Astrophysics, University of Chicago, 5640 S. Ellis Ave, Chicago, IL 60637

⁵ Kavli Institute for Cosmological Physics, University of Chicago, 5640 South Ellis Avenue, Chicago, IL 60637

& Zabludoff 1998; Hashimoto & Oemler 2000). The suppressed star formation in galaxy groups hence will lead to a decline in the mean star formation rate of the Universe as structures grow with decreasing redshift. This scenario provides a plausible explanation for the declining global star formation rate with cosmic time (e.g., Madau et al. 1996; Lilly et al. 1996; Cowie et al. 1999; Cooper et al. 2008).

Within a galaxy group, the properties of galaxies exhibit a dependence on their distance from the group center. Observationally, galaxies in the center of groups are more likely to be bright, red, and early-type. The fraction of early-type galaxies decreases with increasing group-centric radius, while the fraction of fainter, bluer, and late-type galaxies has a positive correlation with group-centric radius (e.g., Domínguez et al. 2002; Brough et al. 2006; Weinmann et al. 2006). Galaxies in the centers of low-mass groups already show different properties from those in the field (e.g., Balogh et al. 2007; Kawata & Mulchaey 2008). Such differences are stronger in higher-mass groups, and galaxies in these groups have properties close to those in clusters (e.g., Domínguez et al. 2002). Galaxy groups, therefore, can be considered as ‘mini-clusters’. Yet galaxy groups are systems typically smaller than clusters by a factor of ~ 10 or more in mass. Mechanisms such as ram-pressure stripping and harassment are perhaps not important within galaxy groups. This makes galaxy groups useful sites to study galaxy evolution possibly free of complicated multiple driving mechanisms.

Most studies on galaxy groups, however, are in the local Universe using samples from the Sloan Digital Sky Survey (SDSS) and the Two-degree-field (2dF) Survey (e.g., Balogh et al. 2004; Martínez & Muriel 2006; Poggianti et al. 2006; Robotham et al. 2006). At $z > 0.1$, our current understanding of galaxy groups is based on samples considerably smaller than that available in the local Universe; for examples, the CNOC2 (e.g., Carlberg et al. 2001; Wilman et al. 2005; Wilman et al. 2005; Balogh et al. 2009), DEEP2 (e.g., Cooper et al. 2007; Gerke et al. 2007), and zCOSMOS (e.g., Knobel et al. 2009; Iovino et al. 2010) group catalogs. Galaxy groups are not easily detected beyond the local Universe because of their low gas content, as well as the less significant number-density contrast to the background. Traditionally, galaxy groups are identified within spectroscopic-redshift samples using algorithms such as the friends-of-friends or the Voronoi tessellation method (e.g., Carlberg et al. 2001; Gerke et al. 2005; Berlind et al. 2006; Söchtig et al. 2006; Tago et al. 2008). The requirement of large spectroscopic surveys with high completeness adds difficulties to the study of galaxy groups at $z > 0.1$, since obtaining such catalogs requires huge amounts of time, money, and work. Another route to identify galaxy groups is to apply dedicated group-finding algorithms to photometric-redshift samples (e.g., Botzler et al. 2004; Li & Yee 2008). Galaxy groups found this way have much larger uncertainties in their redshift estimation, and contain background galaxies as their members. The contamination of false groups may also bias scientific analyses. Even so, the ability to obtain large samples of photometric-redshift galaxy groups will still allow us to gain useful information, after correcting for background contamination statistically.

We study galaxy groups at $0.15 \leq z < 0.52$ using a

photometric-redshift group sample drawn from the multi-band photometric data of the first Red-Sequence Cluster Survey (RCS1; Gladders & Yee 2005). We aim to explore how colors of galaxies, which are a proxy for galaxy population, change with redshift, and how environment affects galaxy populations therein. We follow the methodology used in our study of groups associated with CNOC1 clusters (L09) in deriving photometric redshifts, identifying galaxy groups, and defining environmental parameters. The structure of this paper is as follows. We describe our data and group sample in §2 and §3. The results are presented in §4, and discussed in §5. We summarize our work in §6. We adopt the cosmological parameters $H_0=70$ km/s/Mpc, $\Omega_m=0.3$, and $\Omega_\Lambda=0.7$.

2. THE DATA

2.1. The Observation

We derive our galaxy group sample from the Northern patches of the RCS1, which is an imaging survey with the primary goal of measuring Ω_m and σ_8 using the cluster mass function (Gladders & Yee 2005; Gladders et al. 2007). The survey covers 22 widely separated patches in total in the Northern and Southern sky with a total area of 92 square degrees. The observations were carried out from May 1999 to January 2001. The imaging in R_c and z' of the ten Northern patches was conducted using the CFH-12K camera on the 3.6m CFHT telescope. The camera has $12k \times 8k$ pixels in total, consisting of twelve $2k \times 4k$ CCDs with $0.206''$ per pixel, providing a $42' \times 28'$ field of view. The layout of each patch is arranged with 15 pointings in a slightly overlapping grid of 3×5 pointings, giving a patch size of 2.1×2.3 deg². The integration times are 900 and 1200 seconds with average seeing of $\sim 0.70''$ and $\sim 0.62''$ in the R_c and z' passbands, respectively. The 5σ limiting magnitudes for point sources are $R_c = 24.8$ (Vega) and $z_{AB} = 23.9$ in an aperture of diameter $2.7''$. The details of the data reduction and photometric catalog can be found in Gladders & Yee (2005).

To obtain photometric redshifts, we require additional photometric bands. The B and V photometry for the RCS1 Northern patches was obtained as a follow-up project using the CFH-12K camera (Hsieh et al. 2005). It covers 33.6 deg² in total with 108 pointings ($\sim 75\%$ of the original RCS1-CFHT patches). This defines the sky area used for our group catalog. The runs were carried out from May 2001 to June 2002. The typical exposure times in B and V are 840s and 480s, respectively. The average seeing is $\sim 0.95''$ in B and $\sim 0.65''$ in V . The 5σ limiting magnitudes are $B=25.0$ and $V=24.5$, on average, within an aperture of $2.7''$ diameter. We refer to Hsieh et al. (2005) for more details on the follow-up data set.

2.2. The Photometric-Redshift Catalog

We use the empirical photometric-redshift method modified from Li & Yee (2008) to estimate galaxy redshifts. This photometric redshift algorithm assumes that galaxy redshift is a polynomial function of galaxy magnitudes and colors, and the coefficients are derived from a training set which is a catalog containing spectroscopic galaxy redshifts and multi-band photometry. We construct the redshift training set using spectroscopic samples from the Hubble Deep Field (HDF; Giavalisco et

al. 2004), the Canadian Network for Observational Cosmology Survey (CNOC2; Yee et al. 2000), and the Deep Extragalactic Exploratory Probe (DEEP2; Vogt et al. 2005). The photometry of the training set is processed and calibrated in the same manner as the RCS1 catalogs, and the details can be found in Hsieh et al. (2005). The final training set contains $\sim 5,300$ galaxies with $BVRz'$ photometry.

Instead of dividing the training set and all input galaxies into several fixed color-magnitude cells as was done in Li & Yee (2008), we derive the coefficients of the photometric-redshift polynomial fit individually for each input galaxy by using a subset of the training set which contains 400 galaxies chosen from the complete training set whose magnitudes and colors are the closest to the input galaxy. The choice of the size of the sub-training set is a compromise between accuracy and computation time. Our tests show that any sub-training set with more than 250 galaxies will provide reasonable photometric redshift results. These training galaxies are chosen based on quadratically summed ranks of color and magnitude differences between the training set galaxies and the input galaxy. All four magnitudes and six colors are used. In doing the fitting, we further assign weights to the chosen training-set galaxies, based on the inverse value of their final rank. This partially alleviates the redshift bias that may be introduced to input galaxies near the edges of the color-magnitude distributions. The photometric-redshift errors are estimated empirically by assuming Gaussian magnitude errors and bootstrapping the training set in the color-magnitude cell. We remove galaxies with very large photometric redshift uncertainties from the sample. A galaxy is considered not to have an acceptable photometric redshift if its uncertainty is larger than the very loose criterion of $0.6(1+z)$. As in L09, we assign a weight, w_i , to each galaxy based on the inverse of the fraction of galaxies with acceptable photometric redshifts to the total as a function of R_c magnitude. This w_i is found not strongly dependent on galaxies colors (Yee et al. 2005; Li et al. 2009). The effect of w_i on our results will be further discussed in §5.1.

To test the photometric-redshift accuracy, we randomly exclude 200 galaxies from the training set and treat them as input galaxies. Their photometric redshifts are then derived using the rest of the training set galaxies, and compared with their known spectroscopic redshifts, as presented in Figure 1, along with their estimated uncertainties. For galaxies within our redshift range of interest ($0.15 \leq z_{spec} \leq 0.6$), the overall 1σ dispersion (Figure 1) is ~ 0.064 with a mean $z_{phot} - z_{spec}$ offset set of 0.011. More tests of our photometric-redshift technique using both simulated data and the GOODS-N catalog can be found in Hildebrandt et al. (2010).

3. THE GALAXY GROUP SAMPLE

3.1. Group Catalogs and the Sample

The identification of galaxy groups is achieved using the ‘probability Friends-of-Friends’ (pFoF) algorithm, described and tested in detail in Li & Yee (2008). The algorithm uses the group redshift probability density as a conditional probability density and the photometric-redshift probability distribution of individual galaxies to perform the friends-of-friends linkage in the third dimen-

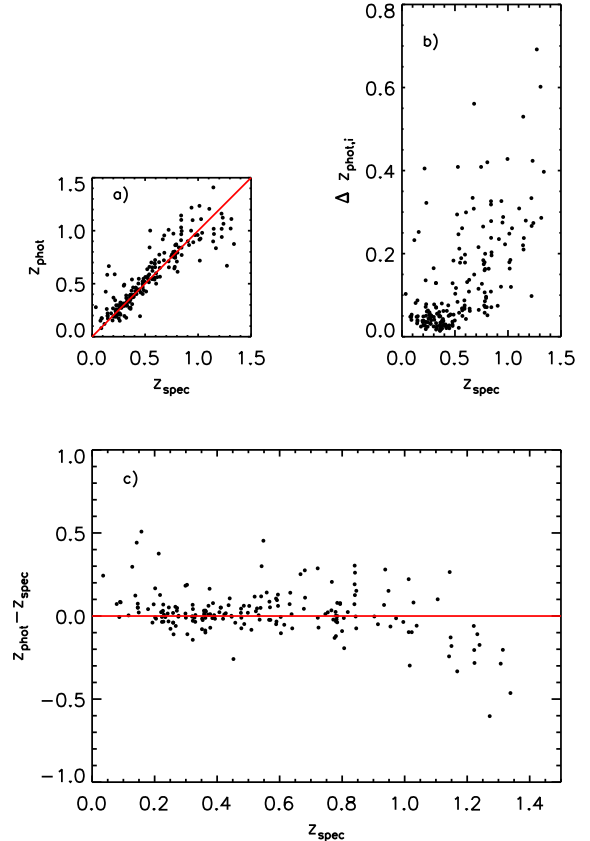


FIG. 1.— Panels a) and c): Comparisons between photometric and spectroscopic redshifts for 200 galaxies whose photometric redshifts are derived using the rest of the ~ 5100 training set galaxies. The 1σ dispersion of $z_{phot} - z_{spec}$ is ~ 0.064 for $0.15 \leq z \leq 0.6$. Panel b): Empirically estimated 1σ photometric redshift uncertainties of individual galaxies as a function of z_{spec} .

sion. A major feature of this algorithm is that the group redshift probability density is improved as more linked group members are added.

The pFoF algorithm has been tested using a simulated catalog (Croton et al. 2006) based on the Virgo Consortium Millennium Simulation (Springel et al. 2005). Different linking criteria in both the 2D sky plane and the redshift direction, as well as various sample depths, have been adopted to investigate the group-finding performance. The results of these tests are described at length in Li & Yee (2008). The RCS group catalogs are obtained by applying the pFoF algorithm to a sample of depth $M_{R_c}^* + 2.0$, where $M_{R_c}^* = -21.41$ (Kodama & Arimoto 1997). We have generated a complete catalog of galaxy groups which is available in electronic form (Table 1). Galaxy groups in this catalog are selected to have $N_{gal} \geq 5$ and $N_{gz} \geq 5$, and redshift between $z=0.15$ and $z=z_{cut}$. Here, N_{gal} is the net weighted member count to $M_{R_c}^* + 2.0$ (i.e., $N_{gal} = \sum(w_i) - N_{bg}$, where the computation of the background counts N_{bg} is presented in §3.5); N_{gz} is the actual number count of the linked galaxies in the pFoF group; and z_{cut} is the redshift where the nominal R_c limit of a patch has a depth of $M_{R_c}^* + 1.5$. The R_c limit is defined as the magnitude at which w_i reaches 2.0, and ranges from 21.16 to 22.86 for the different patches, corresponding to a z_{cut} range of 0.30 to 0.53. The N_{gal}

and N_{gz} limits of ≥ 5 are chosen as a compromise between having a sample reaching down to sufficiently low group mass and the number of false detections, based on the results of our mock tests.

These criteria produce a sample of 1153 groups. Because we use a photometric redshift technique modified from that of Li & Yee (2008), we redo the mock tests for the pFoF algorithm. The results, which are similar to those in Li & Yee (2008), show that this sample may contain $\sim 35\%$ false groups (see §5.1). However, we can use other information to attempt to cut down the fraction of false groups. For examples, the total stellar mass of a group $M_{*,grp}$ and the richness parameter B_{gc} are measured using net M_* and galaxy counts, respectively, within an aperture on the sky, rather than based on FoF connected galaxy counts, and thus provide different information (see §3.4 for the calculations of $M_{*,grp}$ and B_{gc}). Thus, groups with small $M_{*,grp}$ or B_{gc} , and in particular groups with very discrepant $M_{*,grp}$ and B_{gc} (i.e., large B_{gc} small $M_{*,grp}$, or vice versa) are expected to more likely be false groups. This is verified by our mock group sample tests. Applying the same $M_{*,grp}$ cut to the measured $M_{*,grp}$ in our mock catalog, we find that $\sim 65\%$ of the false groups have $\log(M_{*,grp}/M_\odot) \leq 11.2$. For our analyses, we further employ a total group stellar mass cut of $\log(M_{*,grp}/M_\odot) \geq 11.2$ and a richness cut of $B_{gc} \geq 125$ $\text{Mpc}^{1.8} h_{50}^{-1.8}$ in selecting our group sample. The total group stellar mass and richness cuts remove 248 groups from the sample. Assuming that these are mostly false detections, we expect $\sim 15\%$ false groups in the remaining group catalog, which we use as our final group sample. We note that the most significant effect that false groups produce in our analysis is to bias the galaxy red fraction towards smaller values (see §5.1 and Li & Yee (2008)), especially for samples of poor groups where the false detection rate is higher.

We present the basic data of 24 galaxy groups in Table 1 as examples. They are typical groups in each redshift and $M_{*,grp}$ bins in our analyses in §4. Figures 2, 3, and 4 show the sky locations and observed color-magnitude diagrams of these groups. The full sample of 1153 groups is presented in the electronic version of the Table. Some groups are also found as RCS clusters (Gladders & Yee 2005). We note that most groups, especially the richer ones, exhibit a clear red sequence at the expected theoretical model colors.

The redshift distribution of our group sample is plotted in Figure 5. Since different patches have different redshift limits, we also plot in Figure 5 the redshift distribution corrected for the sampling areas for the different redshift bins. For our analysis, we divide the groups into three redshift bins: $0.15 \leq z < 0.35$, $0.35 \leq z < 0.45$, and $0.45 \leq z < 0.52$ designated as the $z \sim 0.25$, $z \sim 0.4$, and $z \sim 0.5$ bins in our analysis. There are 304, 317, and 284 groups, respectively, in these bins.

3.2. Samples of Group Galaxies

To select galaxies in the same redshift space as a group, we follow the method used by L09 for selecting galaxies in the same redshift space as the CNOC1 clusters. That is, the photometric-redshift probability for a galaxy to be at the same redshift as a given group has to satisfy a threshold, which is set to be the same as the redshift

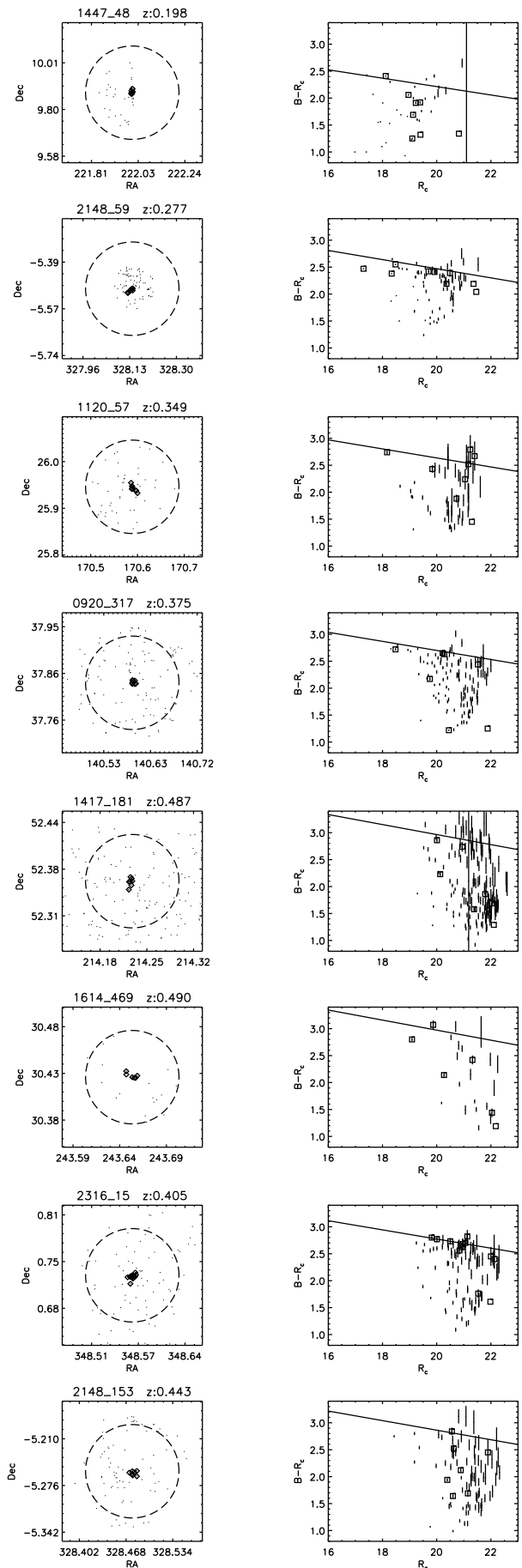


FIG. 2.— Examples of sky locations and observed $B - R_c$ versus R_c color-magnitude diagrams for RCS galaxy groups. The group ID and redshift are indicated in the title of each plot. The circles in the sky maps have a radius of one R_{200} . The linked pFoF members are plotted by squares, while other objects are plotted as dots.

TABLE 1
CATALOGS OF RCS GALAXY GROUPS^a

ID	R.A. ^b	Dec. ^b	z_{grp}	N_{gal}^c	M_{grp}^d	B_{gc}^e
1447_48	14:47:59.4	09:52:46.0	0.198±0.011	6.014	12.45	640±211
2148_59	21:52:33.6	-05:29:24.9	0.277±0.015	7.947	12.45	271±174
1120_57	11:22:17.1	25:58:6.66	0.349±0.019	8.082	12.41	442±211
0920_317	09:22:21.9	37:50:15.7	0.375±0.010	5.486	12.41	653±229
1417_181	14:16:54.0	52:21:29.4	0.487±0.018	6.117	12.41	674±250
1614_469	16:14:36.1	30:25:51.2	0.490±0.014	6.512	12.41	167±203
2316_15	23:14:15.5	00:43:42.8	0.405±0.012	11.18	12.39	685±233
2148_153	21:53:54.8	-05:15:33.7	0.443±0.015	6.341	12.39	454±223
0223_133	02:27:53.7	01:14:10.1	0.207±0.010	5.961	12.02	736±218
1417_23	14:14:35.6	53:54:13.4	0.253±0.008	6.497	12.02	638±205
0920_55	09:23:0.31	37:32:48.4	0.380±0.010	8.591	12.01	808±243
0920_121	09:31:23.5	37:50:9.19	0.503±0.018	9.267	12.01	244±218
0920_365	09:29:2.96	37:49:43.8	0.497±0.017	7.045	12.01	213±213
1614_70	16:13:30.8	30:00:6.82	0.365±0.012	8.067	12.01	443±205
0920_174	09:22:0.56	37:54:28.6	0.418±0.011	6.094	11.96	344±208
0920_322	09:28:5.15	37:55:16.3	0.430±0.017	5.371	11.96	510±226
1614_54	16:17:18.1	30:28:27.9	0.400±0.009	7.978	11.65	366±203
2316_41	23:16:59.4	-00:12:32.5	0.442±0.016	10.36	11.64	395±214
1614_562	16:12:41.3	29:55:42.9	0.491±0.019	5.272	11.62	207±207
1417_321	14:19:0.69	53:51:41.1	0.519±0.023	6.664	11.61	259±223
1447_45	14:46:45.5	10:07:3.18	0.263±0.010	6.237	11.58	188±173
0920_28	09:23:42.5	37:20:13.6	0.220±0.009	5.666	11.57	356±175
0223_252	02:22:19.8	00:05:12.9	0.390±0.011	5.754	11.56	334±205
0223_246	02:25:57.5	00:54:40.9	0.396±0.016	5.206	11.56	264±200

^aThe photometric catalogs are available in Hsieh et al. (2005)

^bin J2000.

^c N_{gal} : net pFoF member count after correcting for background contamination and completeness weights.

^d $M_{grp} = \log(M_{*,grp}/M_{\odot})$, computed using all group members within $0.5R_{200}$ and with background contamination corrected.

^e B_{gc} : computed using all galaxies within 0.25Mpc to the group centers

linking criterion in the pFoF algorithm. These galaxies are called ‘group galaxies’ in our analyses (§4) and are not limited only to the galaxies linked by the pFoF algorithm, since redshift is the only criterion used for their inclusion. In essence, the main task of the pFoF algorithm is to identify the locations where there are groups; the use of the linkage criterion in redshift then generates a sample of galaxies whose photometric redshifts are consistent with being in these groups. In our analyses, we further impose group-centric radius criteria for the selection of group galaxies in various radial bins. We have in total 5028, 5832, and 5560 group galaxies (before background subtraction) brighter than $M_{R_c}^* + 1.5$ within $0.5R_{200}$ (derived from group richness, see §3.3) in the three redshift bins.

We also estimate the stellar mass for each group galaxy using an empirical relation: $\log(M_*/L_{R_c}) = -0.523 + 0.683(M_B - M_{R_c})$, from Bell et al. (2003) with solar units from Worthey (1994). The M_B and M_{R_c} are the k-corrected rest-frame absolute magnitudes derived using the same method as L09. The k-correction values used for each galaxy are based on its color and photometric redshift.

Figure 6 presents the plot of absolute magnitude versus stellar mass for our group galaxy sample. The galaxy sample is complete to $M_{R_c}^* + 1.5$ in all three redshift bins. In stellar mass, the sample is essentially complete to $\log(M_*/M_{\odot})=10.2$ for the $z \sim 0.25$ and $z \sim 0.4$ samples; while the $z \sim 0.5$ sample is 100% complete only to $\log(M_*/M_{\odot}) \sim 10.8$. We note that the level of incompleteness at $z \sim 0.5$ is corrected substantially by the w_i weight assigned to each galaxy. There are a total of 3550, 3933, and 3940 group galaxies within $0.5R_{200}$ with $\log(M_*/M_{\odot}) \geq 10.2$ in the 3 redshift bins, respectively. The number counts for group galaxies at $0.5 \leq R_{200} < 1.0$ are 2637, 3298, and 4605 galaxies for the same redshift divisions.

3.3. Group-Centric Radius and Scaling Radius

To define the center of a pFoF group, we first take the median R.A. and Dec. of all the linked members as the ‘fiducial’ group center. Each linked galaxy is assigned a score based on its R_c magnitude and distance to the fiducial center. The score is then computed as the quadratic sum of the ranks of the magnitude and distance differences between the fiducial group center and the galaxy.

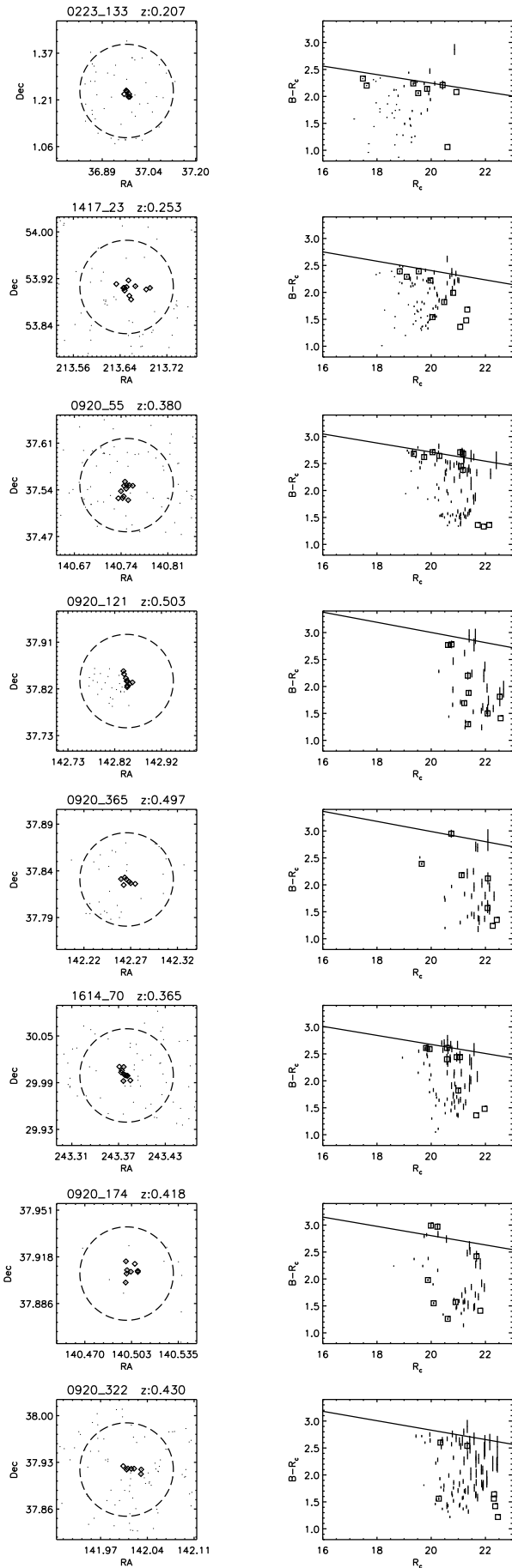


FIG. 3.— Same as Figure 2.

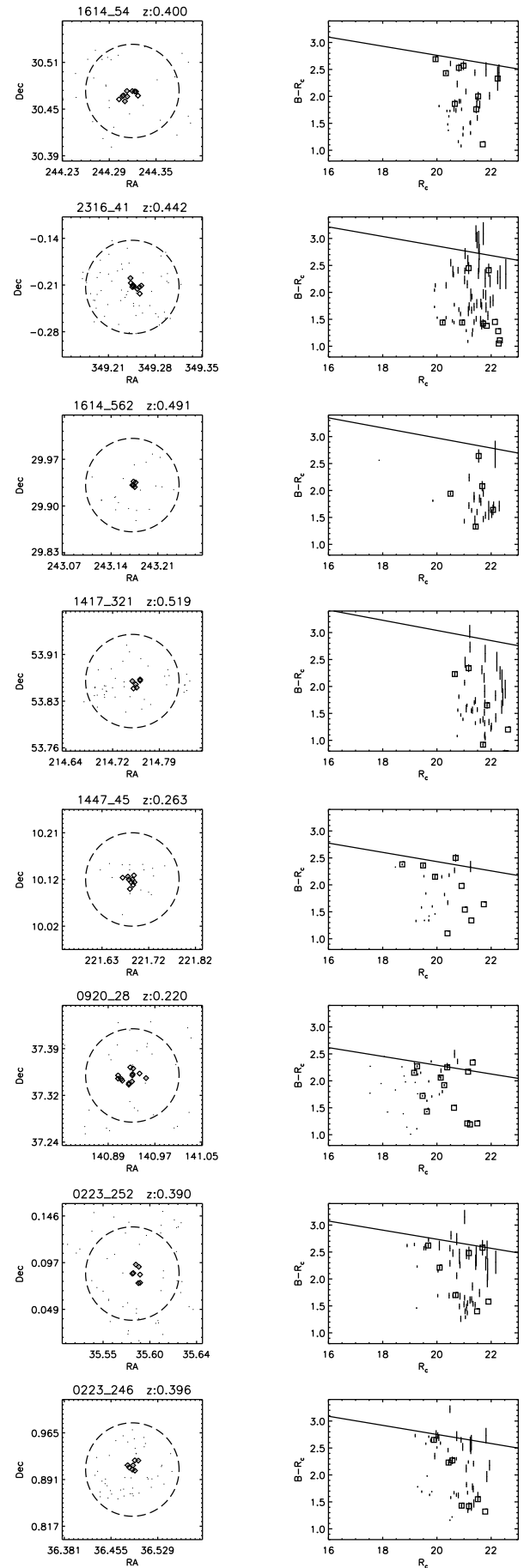


FIG. 4.— Same as Figure 2.

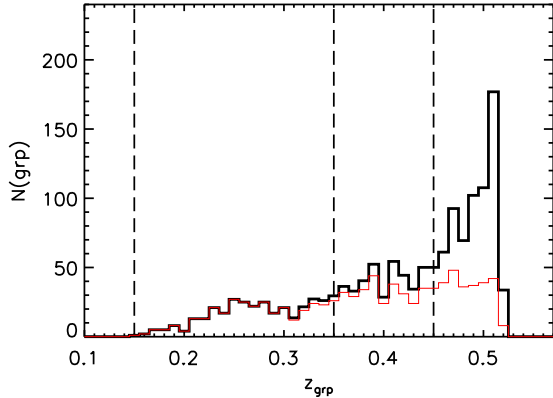


FIG. 5.— The redshift distribution of 905 galaxy groups in our sample using a 0.01 bin size in z . The thin red and thick black histograms are the distributions before and after applying area corrections.

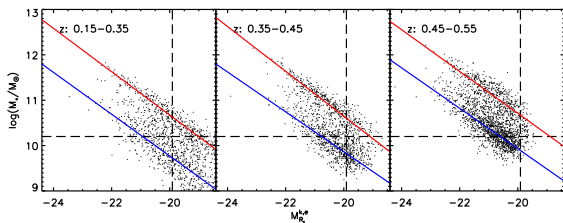


FIG. 6.— Stellar mass M_* and $M_{R_c}^{k,e}$ for group galaxies within $0.5R_{200}$ from 182 groups in the RCS 0920 patch. The vertical dashed line marks $M_{R_c}^* + 1.5$ while the horizontal one, $\log(M_*/M_\odot)=10.2$. The red and blue solid lines mark the ridge lines for red and blue galaxies, respectively. Selecting the sample using stellar mass rejects many blue galaxies.

Both the magnitude and distance contribute the same weight to the score. The galaxy which has the best score is defined as the ‘central galaxy’. We adopt the position of the central galaxy as the final center position of the group from which a group-centric radius is defined. If more than one linked galaxy in the same group has the same score, we choose the center as the one with the brighter magnitude.

For each group galaxy, we compute the projected distance to the center and scale it by R_{200} , the radius within which the density is 200 times the critical density, so that our analysis is not limited only to either the cores of rich groups or the outskirts of poor ones. The R_{200} of each group is estimated from the correlation between cluster richness B_{gc} (see §3.4) and R_{200} derived using the X-ray luminous CNOC1 clusters in Yee & Ellingson (2003) (also see Barkhouse et al. (2007)). The typical R_{200} in our RCS group sample is $\sim 1.07 \pm 0.24$ Mpc. The group-centric radius is denoted by r_{grp} in units of R_{200} . We note that the $B_{gc} - R_{200}$ relation for low-mass galaxy groups may not be identical to that of the CNOC1 clusters, but it still gives us an estimate and rank-order of R_{200} . The effects of the uncertainties in the R_{200} on our results are further discussed in §5.1.3.

3.4. Group Richness and Masses

Galaxy groups and clusters with more members are likely associated with more massive dark matter halos

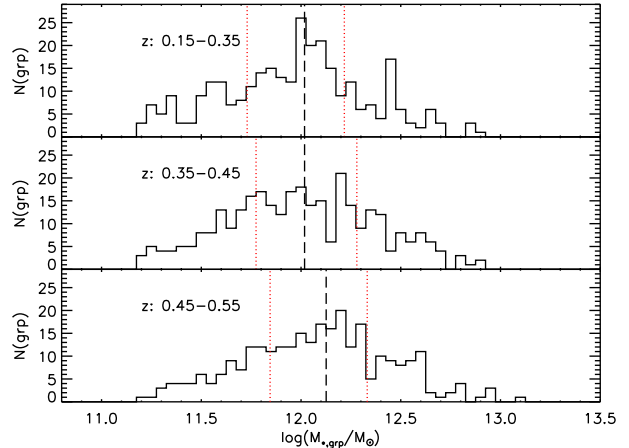


FIG. 7.— The histogram of total stellar mass within $0.5R_{200}$ in each galaxy group. The vertical dashed line is the median value, and the two (red) dotted lines are the 25 and 75 percentiles. The median total group stellar mass remains similar over the three redshift bins.

and have deeper gravitational potentials (e.g., Yee & Ellingson 2003; Popesso et al. 2007). Therefore, to investigate the influence caused by galaxy groups, the group richness should be considered. We explore the parameterization of group richness using two different parameters: the total stellar mass within a fixed fraction of R_{200} and the richness parameter B_{gc} (Longair & Seldner 1979).

We compute the total stellar mass of a galaxy group, $M_{*,grp}$, using the sum of the stellar masses of all the group galaxies within $0.5R_{200}$ in the $\log(M_*/M_{sun}) \geq 10.2$ sample. The $M_{*,grp}$ is corrected for background contamination (see section §3.5). We use $0.5R_{200}$ instead of $1R_{200}$ because group member counts have a larger excess relative to the background within the smaller radius. We note that group galaxies in the $z \sim 0.5$ bin are incomplete at $\log(M_*/M_\odot)=10.2$. However, partly due to the galaxy weight corrections and the small contribution to the total group mass from low-mass galaxies, this has only a few percent effect on the total group stellar mass. This is found to be the case when the incompleteness effect is tested using the average ratios of $M_{*,grp}$ computed with limits of $\log(M_*/M_\odot)=10.2, 10.6,$ and 11.0 for each redshift bin. Figure 7 presents the $M_{*,grp}$ distribution of our group sample in each redshift bin. The distributions are similar for the three redshift bins, peaking at or slightly above $\log(M_*/M_\odot)=12.0$, with median values differing by ~ 0.1 dex. The distributions also show that the sample is beginning to be incomplete at $\log(M_{*,grp}/M_\odot) \lesssim 12$. This is likely due to the pFoF algorithm’s inability to find loose poor groups, and conclusions based on analyses of the low-mass groups should take this bias into consideration.

The B_{gc} parameter is defined as the amplitude of the cluster center-galaxy correlation function, and can be estimated via a deprojection of the angular correlation function onto the spatial one assuming spherical symmetry (Longair & Seldner 1979). It is estimated by counting excess galaxies up to a certain absolute magnitude within a given radius, and is corrected for the background counts and scaled by an average luminosity function and average spatial profile. Details on its computation, robustness as

a cluster richness parameter, and as a mass indicator are presented in Yee & López-Cruz (1999) and Yee & Ellingson (2003).

For the RCS-1 clusters, B_{gc} is computed in a 0.50 Mpc h_{50}^{-1} radius (Gladders & Yee 2005). Considering that galaxy groups are poorer systems than galaxy clusters, we calculate B_{gc} for each galaxy groups using a 0.25 Mpc h_{50}^{-1} radius to minimize background noise. We find that the B_{gc} values computed using a radius of 0.50Mpc are $\sim 35\%$ smaller than those using a 0.25Mpc radius, indicating a steeper slope of the galaxy correlation function than the canonical $\gamma = 1.8$. We note that a cluster of $B_{gc} = 600\text{Mpc}^{1.8}h_{50}^{-1.8}$ (within a radius of 0.5Mpc) has a richness equivalent to Abell class 0, or a mass of $\sim 3 \times 10^{14}h^{-1}M_{\odot}$ (Yee & Ellingson 2003).

Figure 8 presents the comparison between B_{gc} and $M_{*,grp}$. A positive correlation is observed, with the scatter broadly consistent with the measurement errors. We obtain the best fitting power-law, using the more robust $N_{gal} \geq 8$ sample: $\log(M_{*,grp}/M_{\odot}) = 1.41\log(B_{gc}) + 8.30$. Using the simple scaling relations in Yee & Ellingson (2003) with the assumption that galaxies trace total halo mass, we should expect the halo mass within a dynamically scaled radius (e.g., M_{200} , the mass within R_{200}) to scale as $B_{gc}^{3/\gamma}$, where γ is the power-law slope of the galaxy-galaxy correlation function; or, for the canonical γ of 1.8, $\log(M_{200}) \sim B_{gc}^{1.66}$. Thus, our power-law fit of $M_{*,grp}$ and B_{gc} is consistent with $M_{*,grp}$ being a direct one-to-one proxy for the M_{200} halo mass of the groups. Using the correlation from Yee & Ellingson (2003) between B_{gc} and M_{200} , and compensating for H_0 , we can roughly estimate the relation between the total group stellar mass and the halo mass. We do this by fitting the $M_{*,grp}-B_{gc}$ relation using the same power-law slope (1.64) as that measured by Yee & Ellingson (2003) for the $M_{200}-B_{gc}$ relation for the CNOC1 clusters, and correcting for factor of 0.65 in B_{gc} values computed using a 0.5 h_{50}^{-1} Mpc radius. This gives $\log(M_{200,grp}) \sim \log(M_{*,grp}) + 1.85$. This provides a very rough scaling, probably no better than a factor of two, between the group stellar mass and M_{200} . In this scaling, a group with $\log(M_{*,grp}/M_{\odot}) = 12.0$, (approximately the median $M_{*,grp}$ for our sample), represents a halo mass of $\sim 7 \times 10^{13}M_{\odot}$. In the remainder of the paper, we use the group stellar mass $M_{*,grp}$ as the richness indicator and a rough halo mass proxy.

3.5. Background Correction

Because of the relatively large uncertainty of the photometric redshift, even with the use of the pFoF algorithm for determining whether a galaxy belongs to a given group, there will still be a significant fraction of “group galaxies” which are field, or near-field, galaxies, especially at the larger group-centric radii. Hence, it is essential to perform background contamination corrections in analyses using the group galaxy sample. We construct both luminosity-limited and stellar-mass-selected samples of background counts using three RCS patches: 0920, 1417, and 1614. These three patches have the deepest photometry and cover a total of 11.38 deg² on the sky. We note that these three control patches are part of our whole sample. The deep photometry allows

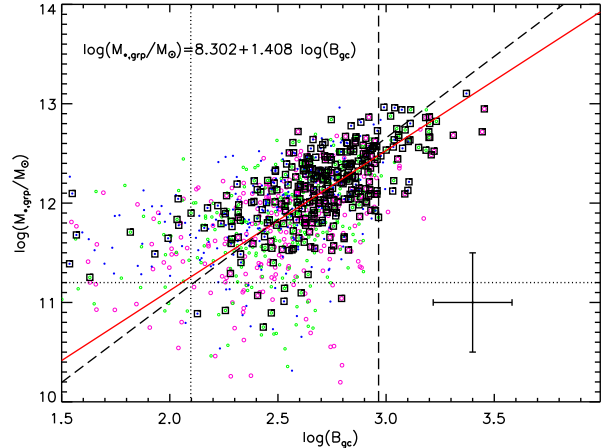


FIG. 8.— The comparison between $M_{*,grp}$ and B_{gc} , two parameters used as indicators of group richness. A correlation is seen. The dotted lines indicate the $B_{gc}=125$ and $\log(M_{*,grp}/M_{\odot})=11.2$ criteria for selecting our final group sample. The solid line is the linear fit (displayed on the top of the figure) between $\log(M_{*,grp}/M_{\odot})$ and $\log(B_{gc})$ using groups with $N_{gal} \geq 8$, while the dashed line is the fitted relation using a slope of 1.64 (the slope obtained by Yee & Ellingson (2003) fitting M_{200} vs B_{gc} for a sample of CNOC1 clusters). The vertical dashed line marks the mass of $M_{200} \sim 3 \times 10^{14} M_{\odot}$, based on the calibration of Yee & Ellingson. Galaxy groups are represented by circles, with larger symbols representing groups at lower redshift. Squares mark groups with linked pFoF members $N_{gal} \geq 8$. The error-bars on the lower right represent typical uncertainties in the two parameters.

us to compute galaxy counts to a higher redshift.

We use the method in L09 to construct the galaxy number surface density per Mpc² in the field in redshift bins of $\Delta z = 0.01$, denoted as $n(z, M_{R_c})$ and $n(z, M_*)$. Briefly, the $n(z)$ functions are obtained by integrating the sum of weighted photometric redshift probability densities of all galaxies in the three patches within each small redshift interval and normalized by the area of the patches. For a given set of galaxies, e.g., a sample of group galaxies within certain group-centric radius over certain magnitude range, the total number of background galaxies is computed by multiplying the appropriate $n(z)$ curve with the summed photometric-redshift likelihood function of all galaxies of interest, normalized by the area. A more detailed description of the method can be found in L09.

3.6. Local Galaxy Density

It has been shown that local galaxy density plays a role in transforming star-forming galaxies into passive ones (e.g., Gómez et al. 2003; Goto et al. 2003). We compute local galaxy density Σ_5 based on the nearest 5th neighbor galaxy for each group galaxy using the ‘group galaxies’ in our two samples. The Σ_5 is then corrected for background galaxy contamination (see L09 for more details of the computation). The Σ_5 is computed using galaxies brighter than $M_{R_c}^* + 1.5$ for the luminosity-limited sample, and using galaxies with $\log(M_*/M_{\odot}) \geq 10.2$ for the stellar-mass-selected sample. We note that in general blue galaxies in the stellar-mass-selected sample have somewhat smaller Σ_5 than those in the luminosity-limited sample, and the differences are primarily seen in low Σ_5 regions. This is because most blue galaxies in the luminosity-limited sample have stellar mass less than $\log(M_*/M_{\odot}) = 10.2$, and they are excluded in the

stellar-mass-selected sample.

3.7. Red Galaxy Fraction

As the red sequence of early-type galaxies is the final destination for galaxies on a color-magnitude diagram, we probe the dependence of the red galaxy fraction, f_{red} , with various group properties. The f_{red} is computed based on the same method as L09 but using samples of galaxies defined by stellar-mass limits. The red galaxies are defined as those whose colors are redder than half the color differences between the spectral energy distributions (SEDs) of E/S0 and Sc galaxies at a given redshift, which is tabulated in Poggianti (1997). This color division changes with redshift on an observed color-magnitude diagram, and follows the passive evolution of galaxy colors. The color division is typically 0.25 to 0.30 mag to the blue of the red sequence, and is comparable to the $\Delta B - V = 0.2$ used by Butcher & Oemler (1984), and the definition used by Ellingson et al. (2001). The background count corrections for the red galaxy counts are derived using the method described in §3.5 but applied to background galaxies with the color cut described above. We compute f_{red} using a statistical inference (D’Agostini 2004; Andreon et al. 2006) because the background contamination plays a role in estimating the true fraction of red group members especially when the number of galaxies in a group is not large.

4. RESULTS

In the following subsections, we investigate f_{red} as a function of redshift, $M_{*,grp}$, r_{grp} , and Σ_5 . We have explored results using both the luminosity and stellar-mass samples. We find that both samples exhibit consistent trends and lead to similar conclusions. We therefore present and discuss our results using only the stellar-mass selected sample. We note that, as discussed in L09, using a luminosity-selected galaxy sample is equivalent to having different stellar-mass limits for the red and blue galaxies. Our luminosity-selected sample has equivalent stellar-mass limits of $\log(M_*/M_\odot) \sim 10.5$ and $\log(M_*/M_\odot) \sim 9.8$, for red and blue galaxies (Figure 6), respectively. On the other hand, the nominal stellar-mass limit of $\log(M_*/M_\odot) = 10.2$ of the stellar-mass selected sample corresponds to $M_{R_c}^{k,e} \sim -19.0$ and -20.75 , for red and blue galaxies, respectively. Thus, for the $z \sim 0.5$ bin the red group galaxy sample is substantially incomplete at $\log(M_*/M_\odot) = 10.2$, and we include results from the $z \sim 0.5$ bin only for samples with a stellar-mass limit of $\log(M_*/M_\odot) \geq 10.6$.

To investigate the dependence of galaxy population on group richness or mass, we also divide our group sample into high-, intermediate- and low-mass bins of $\log(M_{*,grp}/M_\odot) \geq 12.2$, $12.2 > \log(M_{*,grp}/M_\odot) \geq 11.8$, and $11.8 > \log(M_{*,grp}/M_\odot) \geq 11.2$. These bins correspond to, approximately, $M_{200} \geq 1.1 \times 10^{14} M_\odot$, $1.1 \times 10^{14} M_\odot > M_{200} \geq 4.5 \times 10^{13} M_\odot$, and $4.5 \times 10^{13} M_\odot > M_{200} \geq 0.7 \times 10^{13} M_\odot$, respectively. We intend to probe f_{red} out to $r_{grp} \sim 2$. Due to the less accurate redshift information in photometric redshifts, a small number of galaxies may belong to more than one group. In this situation, we re-assign the galaxy’s group membership to the group for which the group-centric radius is the smallest.

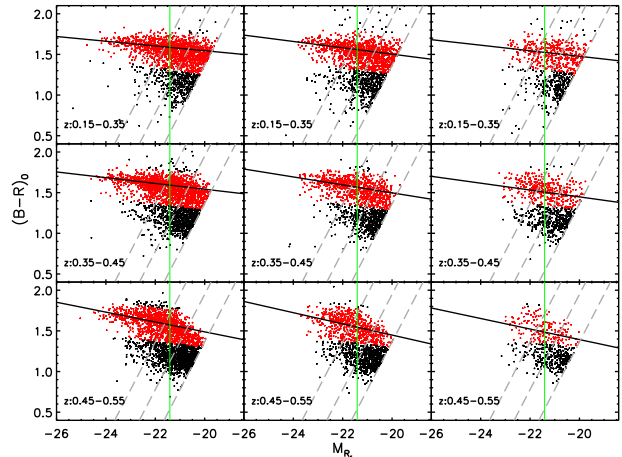


FIG. 9.— Stacked rest-frame $B - R$ vs M_{R_c} for group galaxies within $0.5R_{200}$ in each redshift and $M_{*,grp}$ bin. The gray dashed lines in each panel mark $\log(M_*/M_\odot) = 11.0, 10.6,$ and 10.2 from left to right. The vertical green line is $M_{R_c} = 21.41$. Red dots represent galaxies satisfying the definition of red galaxies as described in §3.7. The solid lines are the fitted red sequences using red galaxies with $\log(M_*/M_\odot) \geq 10.6$. The fitting results are listed in Table 2. Group galaxies, including those in poor groups, exhibit similar color-magnitude relations as those in clusters.

4.1. Color-magnitude Diagrams and the Red-Sequence for Group Galaxies

Figure 9 presents the stacked rest-frame color-magnitude diagrams for group galaxies within $0.5R_{200}$ at each redshift and $M_{*,grp}$ bin. We do not apply any background correction in Figure 9, but the contamination of background galaxies is not expected to be large for reasonably luminous galaxies, since these group galaxies are already pre-selected by photometric redshift and a relatively small group-centric radius is used. The very small number of galaxies in the CMDs redder than the red-sequence indicates that the contamination rate is small. We find that group galaxies exhibit color-magnitude distributions similar to clusters: that is, group galaxies can be separated into two distinct populations of red and blue galaxies, and the red members, including those in poor groups, form a clear sequence.

We fit the red sequence using red galaxies with $\log(M_*/M_\odot) \geq 10.6$, and present the resulting fit in Table 2. We use a relatively high stellar-mass limit to perform the fit to minimize possible confusion arising from the blue cloud galaxies due to larger photometric uncertainties at the faint end. These red group galaxies are defined in the same manner as described in §3.7. We further impose a red-cut of 0.3 mag redder than the model red-sequence color, in order to minimize the effect on fitting from the small number of galaxies in the group galaxy sample which are likely background galaxies with colors significantly redder than the red sequence model. Because of the more sparse data for the low stellar-mass groups, we fix the fitting slope for these groups to be that of the average of the two bins of the more massive groups at the same redshift to derive the red-sequence colors and dispersion. We find that the slopes and zero points of the fitted red sequences are similar among different redshift and $M_{*,grp}$ bins – an indication that the formation epochs for $\sim M^*$ galaxies in these groups are typically at $z \gtrsim 2$ (e.g., Stanford et al. 1998; Gladders et al.

TABLE 2
THE FITTED CMR FOR FIG.9
IN THE FORM AS $y = A + Bx$ OR $y = C + B(x+21.41)$

z	$M_{*,grp}$	A	B	C
0.00–0.35	12.2–14.0	0.963 ± 0.049	-0.029 ± 0.002	1.584
0.00–0.35	11.8–12.2	0.723 ± 0.068	-0.039 ± 0.003	1.558
	11.2–11.8	0.796 ± 0.001	-0.034*	1.524
0.35–0.45	12.2–14.0	0.834 ± 0.039	-0.035 ± 0.002	1.583
0.35–0.45	11.8–12.2	0.520 ± 0.098	-0.049 ± 0.004	1.569
	11.2–11.8	0.605 ± 0.002	-0.042*	1.504
0.45–0.55	12.2–14.0	0.274 ± 0.075	-0.061 ± 0.003	1.580
0.45–0.55	11.8–12.2	0.071 ± 0.162	-0.069 ± 0.007	1.548
	11.2–11.8	0.098 ± 0.005	-0.065*	1.490

* using the mean slope of the other two $M_{*,grp}$ bins at the same redshift.

1998). The average slope of ~ -0.046 for the 6 more massive group samples is consistent with the value of -0.047 in the model of Kodama & Arimoto (1997). We see a consistent trend of increasing slope, by about -0.03 from the $z = 0.25$ to $z = 0.5$ bins, which is entirely in agreement with that observed for clusters over this redshift range (but for slightly different filters) in Gladders et al. (1998, see their Figure 4) and their models.

The average red-sequence rest-frame zero point ($B - R_c$)₀ at $M_{Rc}^* = -21.41$ is 1.570 mag, and has a small root-mean-squared (rms) dispersion of 0.016 mag over all redshifts and $M_{*,grp}$ bins. However, it appears that there is a trend of a slightly bluer ($B - R_c$)₀ zero point for less massive groups: The zero points averaged over redshift are 1.571, 1.576, and 1.564 for the massive-, intermediate-, and low-mass group samples. These differences account for almost all the dispersion in the red-sequence color zero points, as the variations over redshift within each group mass grouping are only $\sim \pm 0.01$ mag. It is not clear whether this small observed difference is a reflection of a trend in the average age since formation or the average metallicity in the luminous red-sequence galaxies in groups of different masses.

We also compute the dispersion of the rest-frame $B - R_c$ colors for the bright ($\leq M^*$) red-sequence galaxies in the 9 subsamples. They range from 0.08 to 0.10 at the low- and high-redshift bins for the more massive groups, to about 0.10 for the low-mass groups at all redshift bins. However, there are two observational uncertainties which contribute to the dispersion of the red-sequence. First, the photometric redshifts of the groups have a typical uncertainty of 0.03, which translates into an uncertainty of about 0.03 mag in the k-corrections for red galaxies. Second, the typical mean photometric uncertainties in $B - R_c$ range from 0.03 mag for the low-redshift samples (at the brighter end of our photometry) to 0.06 mag for the high-redshift samples. Rough corrections in quadrature for the dispersion due to these effects give the intrinsic red-sequence color dispersion to be ~ 0.03 for all cases. While the rough corrections and the possible contamination from background galaxies prevent us from discerning any pattern in the red-sequence dispersions for the different subsamples, the estimated average dispersion is consistent with observations of much smaller samples of rich clusters with more precise redshift and

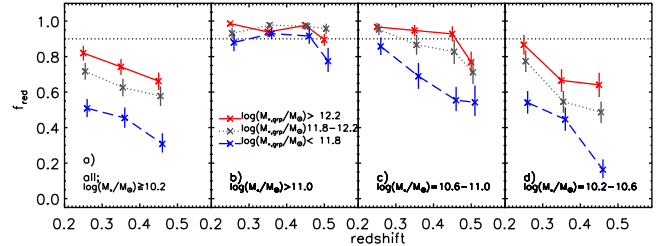


FIG. 10.— Red-galaxy fraction, f_{red} , as a function of redshift in three $\log(M_{*,grp})$ bins using all groups galaxies within $0.5R_{200}$ without and with stellar mass controlled. Groups with larger $M_{*,grp}$ exhibit larger f_{red} , indicating an apparent group down-sizing effect.

photometric information (e.g., Sandage & Visvanathan 1978; Bower et al. 1992; Ellis et al. 1997)

This high degree of uniformity in the red sequence in our group samples suggests that the more massive ($\sim M_{Rc}^*$, or $\log(M_*/M_\odot) \geq 11.0$) red-sequence galaxies are very similar by $z \sim 0.5$ in all groups with a halo mass larger than approximately $10^{13.5} M_\odot$; i.e., their formation time is likely to be at $z \geq 2$, similar to the conclusions drawn from more massive clusters (e.g., Gladders et al. 1998; Quadri et al. 2007). From a visual inspection of the CMDs, the number of blue group galaxies appear to drop significantly from $z \sim 0.50$ to $z \sim 0.25$. In the next section, we quantitatively measure the fraction of red group member galaxies (f_{red}) and examine their dependence on group and galaxy properties.

4.2. Dependence of f_{red} on Group Total Stellar Mass

We probe the red galaxy fraction f_{red} in galaxy groups, computed within $0.5R_{200}$, as a function of redshift for the three different $M_{*,grp}$ samples and present the results in Figure 10. Panel a) of Figure 10 shows the change in f_{red} as a function of redshift to $z = 0.45$ using a galaxy stellar-mass limit of $\log(M_*/M_\odot) = 10.2$. Note that we measure f_{red} only out to $z \sim 0.45$, as at $z \sim 0.5$ the galaxy sample is not complete at the $\log(M_*/M_\odot) = 10.2$ level. All three $M_{*,grp}$ subsamples exhibit increasing f_{red} toward lower redshift; i.e., the Butcher-Oemler effect (Butcher & Oemler 1984) observed on the scale of galaxy groups. The more massive groups have a larger f_{red} in all redshift bins. In other words, more massive groups turn their galaxies red, due to the suppression of star formation activity, at an earlier time than those in less massive groups. This result can be described as a down-sizing evolution effect of sorts operating in galaxy groups.

To ascertain that this effect is not the result of relatively more massive galaxies inhabiting more massive groups, we further control for the stellar mass of group member galaxies in the next three panels of Figure 10. To aid in the discussion of the evolution of f_{red} , we use $f_{rT} = 0.85$ as the threshold f_{red} for which a sample of galaxies is considered as having the bulk of its galaxies with their star formation quenched. Panel b) shows that the most massive group member galaxies ($\log(M_*/M_\odot) > 11$) exhibit essentially flat $f_{red}-z$ trends for groups in different $M_{*,grp}$ bins with $f_{red} > f_{rT}$, with the exception of the $z \sim 0.5$ point for the low-mass groups. That is, these massive group galaxies have mostly finished their star formation by $z \sim 0.5$, regard-

less of the influence of group environment.

In contrast, the effect of $M_{*,grp}$ is clearly observed for the subsamples of galaxies of intermediate and low stellar masses. First, galaxies of similar stellar masses are redder in more massive groups (panels c and d), regardless of redshift, demonstrating the dependence on $M_{*,grp}$. Second, the $f_{red}-z$ trends are different for intermediate- and low-mass galaxies in groups of different $M_{*,grp}$. The intermediate-stellar-mass galaxies in the massive groups reach f_{rT} at z between 0.45 to 0.25, depending on the mass of the groups to which the galaxies belong. For the low-stellar-mass galaxies, only those in the most massive groups manage to barely reach f_{rT} at $z \sim 0.25$. In general, the low-mass galaxies also show larger changes in f_{red} than the intermediate-stellar-mass galaxies over $z \sim 0.45$ to $z \sim 0.25$ range. The different behaviors of the $f_{red}-z$ trends for these three subsamples indicate that, while the f_{red} correlates strongly with the stellar mass of the group galaxies, the halo mass of the group in which the galaxies are situated also has a significant influence on the evolution of the lower-mass group galaxies. Galaxies in higher mass groups reach f_{rT} at an earlier epoch and have a less steep $f_{red}-z$ trend.

The large f_{red} and flat trends with redshift for the massive group galaxies further provides evidence of galaxy ‘down-sizing’ studied in the literature; i.e., star formation takes place and also stops earlier in massive galaxies, then shifts to less massive systems at later times (e.g., Cowie et al. 1996; Cattaneo et al. 2008; Seymour et al. 2008). Massive galaxies, by and large, show little effect from being in groups of different masses (at these moderate redshifts); their evolutionary stage is likely a reflection primarily of their own mass. However, lower-mass galaxies do show evolutionary histories significantly correlated with the halo mass of their parent groups. Hence, the ‘group down-sizing’ observed in panel a) of Figure 10 is not caused by differences in the stellar mass distributions of member galaxies in groups with different richness, but rather is the result of lower-mass member galaxies in higher-mass groups being in a more advanced evolutionary state than those in lower-mass groups.

4.3. Dependence of f_{red} on Group-Centric Radius

In the literature, many studies have suggested that group environment can truncate star formation in their member galaxies (e.g., Font et al. 2008; Verdugo et al. 2008; van den Bosch et al. 2008; Wilman et al. 2008, L09). For example, Domínguez et al. (2002) have shown, using groups from the 2dF, that the fraction of galaxy populations in groups, especially the rich and massive ones, exhibit similar radial trends as those observed in galaxy clusters with an offset in the values of f_{red} . Using the CNOC2 group catalog, Wilman et al. (2005) found that the fraction of passive spiral galaxies, which are galaxies of spiral morphology but with no/little [OII] emission lines, increases continuously toward the group center, and demonstrate that star formation rate is truncated gradually as galaxies move toward the group center.

To quantify radial color trends within galaxy groups, we compute f_{red} as a function of r_{grp} . We separate the group sample by group total stellar mass $M_{*,grp}$, since we have found in §4.2 that the f_{red} within groups at a fixed redshift depends on $M_{*,grp}$. The results, using group galaxy samples with a stellar mass limit of $\log(M_*/M_\odot) \geq$

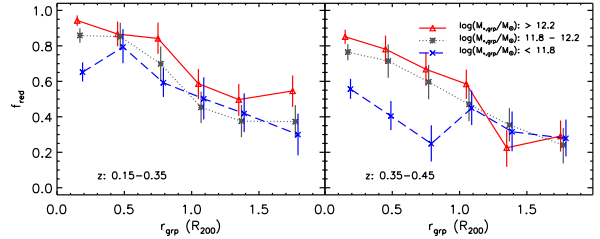


FIG. 11.— Red-galaxy fraction f_{red} as a function of group-centric radius r_{grp} in units of R_{200} by stacking all group galaxies in each bin. Groups are separated into three richness bins indicated in the plot. The f_{red} decreases with r_{grp} . The differences in f_{red} among groups of different richness are seen primarily within the virialized region ($r_{grp} < 1$).

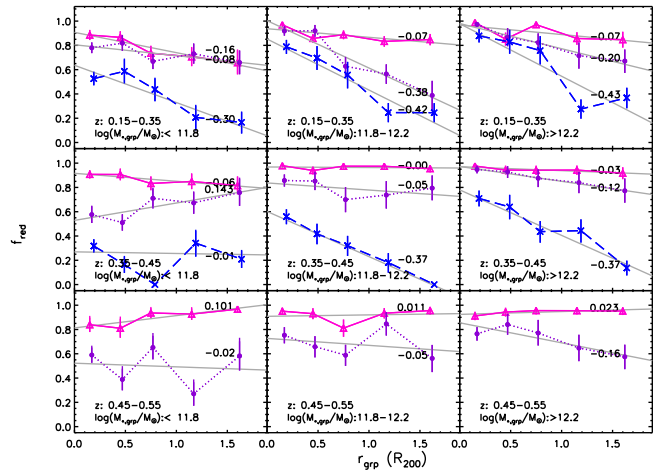


FIG. 12.— ‘ $f_{red}-r_{grp}$ ’ trends for group galaxies with $\log(M_*/M_\odot) > 11.0$ (solid pink), $\log(M_*/M_\odot)=10.6-11.0$ (dotted purple), and $\log(M_*/M_\odot)=10.2-10.6$ (dashed blue) in each redshift and $\log(M_{*,grp})$ bin as indicated in the panels. A simple linear fit is applied to each trend with the slope indicated. In general more massive group member galaxies exhibit gentler slopes toward to the center, and more massive groups produce steeper radial dependence.

10.2 are presented in Figure 11 for the two lower redshift bins.

Generally speaking, group galaxies in all $M_{*,grp}$ and redshift bins exhibit declining f_{red} with increasing r_{grp} . The central regions of the groups are dominated by red members with $f_{red} \sim 0.6$ to 0.9 , dropping to $\sim 0.3-0.4$ at the outskirts. For both redshift bins, the effect of $M_{*,grp}$ is clearly observed within $r_{grp} \lesssim 1$, where groups of higher $M_{*,grp}$ have larger f_{red} . Beyond R_{200} , the differences in f_{red} among different $M_{*,grp}$ groups become smaller, and approaching similar values of $f_{red} \sim 0.3$ to 0.4 for all groups. However, the observed trends in Figure 11 are likely driven differently by group galaxies of different stellar masses. We accordingly re-plot the $f_{red}-r_{grp}$ trends by dividing our group galaxies into three subsamples, with $\log(M_*/M_\odot) > 11.0$, $\log(M_*/M_\odot) = 10.6 - 11.0$, and $\log(M_*/M_\odot) = 10.2 - 10.6$. For the two subsamples of more massive galaxies, we also include the $z \sim 0.5$ redshift bins. The results are presented in Figure 12. As an aid to interpretation, we also perform linear fits of the $f_{red}-r_{grp}$ trends for the 24 subsamples, with the best fitting slopes shown in the Figure.

While the error bars are large for these plots, several trends are apparent. As expected, the most massive

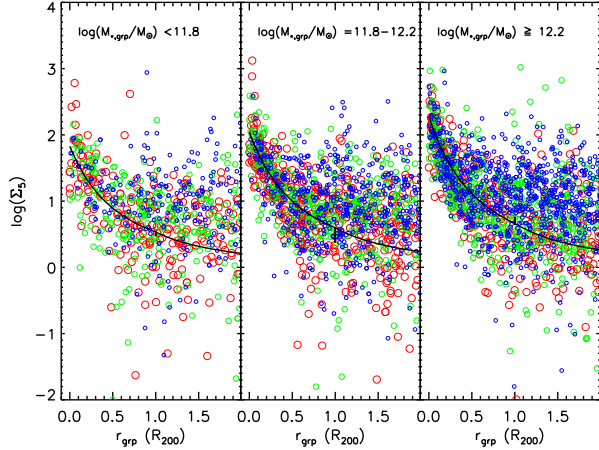


FIG. 13.— Local galaxy density Σ_5 as a function of r_{grp} in groups with different $M_{*,grp}$. Larger circle sizes indicate galaxies at lower redshift. The solid curves are the fitted 2D NFW (Navarro et al. 1996) relations using the analytic form in Bartelmann et al. (1996).

galaxies ($\log(M_*/M_\odot) > 11$) show little effect from their location within their parent group, as almost all have essentially $f_{red} \geq f_{rT}$. The changes in the $f_{red}-r_{grp}$ trends with z or $M_{*,grp}$ are primarily driven by group galaxies with intermediate ($10.6 \leq \log(M_*/M_\odot) < 11.0$), and low masses ($10.2 \leq \log(M_*/M_\odot) < 10.6$). These $f_{red}-r_{grp}$ trends follow a couple of general patterns. First, the low-mass galaxy samples have the steepest radial changes of f_{red} for all group mass and redshift bins, indicating that they are affected by the group environment the most. Second, the radial slope of f_{red} appears somewhat shallower for these galaxies in low-massive groups, which is suggestive that more massive halos may have a relatively larger effect on the galaxies that they are accreting, although larger samples are needed to verify this effect.

4.4. Local Galaxy Density for Group Galaxies

It has generally been accepted that local galaxy density can affect galaxy properties such as star formation rates and colors (see §1). Using a small sample of rich clusters, L09 probed the local galaxy density effect on cluster galaxies at different cluster-centric radii over $0.15 < z < 0.55$. They showed that local galaxy density has an important effect at cluster outskirts but less so in the cluster central regions. Here, with a much larger sample covering a larger range of halo masses, we examine the interplay between the local galaxy density effect and group environmental influence, as parameterized by the group-centric radius, on group galaxies. These two measures can be considered different in that the former tells us how close neighbors affect the galaxy population, while the latter delineates the effect due to the position of the galaxy in the larger parent halo.

Figure 13 plots the local galaxy density, Σ_5 , for each group galaxy, which is measured based on the nearest fifth neighbor distance using the method in L09, as a function of the group-centric radius for groups with different $M_{*,grp}$. The distributions cover over three orders of magnitude in local density and can be described in general as having a decreasing average with increasing radius. In each $M_{*,grp}$ bin, we also show that the local density distribution roughly follows a projected NFW

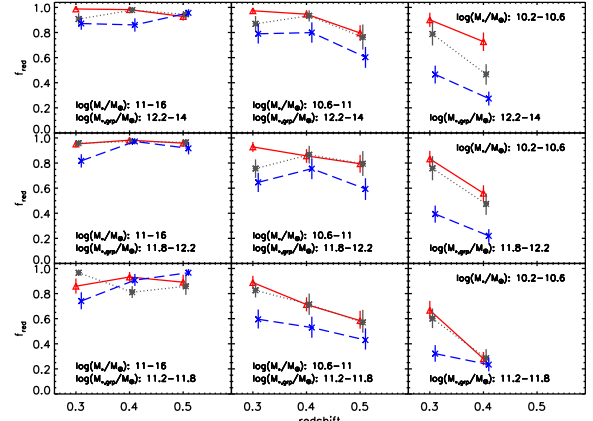


FIG. 14.— Red-galaxy fraction f_{red} within $1.5R_{200}$ as a function of redshift for galaxies in different local galaxy density Σ_5 subsamples. The 9 panels separate subsamples of different group stellar masses $M_{*,grp}$ and galaxy stellar masses M_* , as indicated on each panel. The red solid, gray dotted, and blue dashed curves represent high-, intermediate-, and low- Σ_5 divisions, respectively.

profile (Navarro et al. 1996), fitted following the prescription of Bartelmann et al. (1996). These plots show that the Σ_5 measurement produces meaningful relative local density information when the density range is sufficiently large, e.g., over a factor of several from low to high density. Typically, the group core has local galaxy densities that are close to 100 to several hundred times higher than those at $2R_{200}$, for low- and high-mass groups, respectively. Within $0.5R_{200}$, Σ_5 decreases smoothly with r_{grp} . Beyond that, some regions with higher Σ_5 are super-imposed on the envelope, indicating possible infalling sub-groups at large r_{grp} , or the ambiguity in group membership among multiple groups.

4.4.1. The Effect of Local Density

To examine the effect of local galaxy density environment on the galaxy population, in Figure 14 we plot f_{red} as a function of redshift for group galaxies within $1.5R_{200}$ into three bins of local galaxy density. We further separate the galaxy samples into bins of galaxy stellar mass and total group stellar mass as in §4.3, since we have found that f_{red} has a dependence on both of these parameters. Figure 14 provides a look at the effect of Σ_5 integrated over the whole group. Our highest and lowest Σ_5 bins contain the highest 20-percentile and the lowest 40 percentile of group galaxies in our sample. The median local galaxy density values of the high- and intermediate-density bins are approximately 12.8 and 3.7 times that of the low-density bin, respectively.

The main feature of Figure 14 is that the effect of Σ_5 depends on galaxy stellar mass. Within the factor of ~ 13 between the low- and high-density bins, f_{red} increases by ~ 0.2 for the intermediate-mass galaxies, and ~ 0.4 for the low-mass galaxies; whereas for the high-mass galaxies, there is no statistically significant difference in f_{red} . The trends for the high- and intermediate-mass galaxies appear to be very similar for galaxies in groups of different $M_{*,grp}$, and also over the redshift range of 0.5 to 0.25. For the low-mass galaxies, the differentials in f_{red} due to different Σ_5 may be somewhat larger for galaxies in massive groups. Thus, the magnitude of the local galaxy density effect appears to be

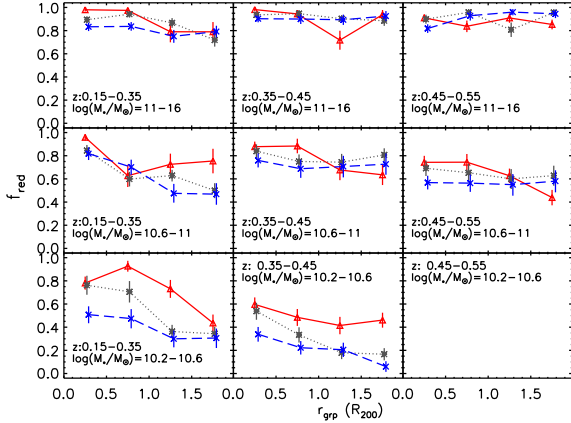


FIG. 15.— Red-galaxy fraction f_{red} as a function of group-centric radius r_{grp} for group galaxy subsamples of different local galaxy density Σ_5 . The subsamples are further divided by redshift and group member galaxy stellar mass M_* bins, as indicated on each of the 8 panels. The different Σ_5 subsamples from high to low are plotted in different linestyles as (red) solid, (gray) dotted, and (blue) long-dashed, respectively. Groups of all total group mass $M_{*,grp}$ are combined for better signals.

fairly similar for galaxies in groups of different richness across the redshift range of 0.5 to 0.2, but has a strong dependence on the stellar mass of the galaxies.

4.4.2. Local Galaxy Density and Group Environment

The parameters Σ_5 and r_{grp} are correlated. To examine how these two effects interplay with each other, in Figure 15 we present f_{red} of samples of group galaxies of different stellar masses as a function of r_{grp} for galaxies in three Σ_5 environments at different redshifts. Since it appears that the group halo mass has only a weak influence on the effect of Σ_5 on f_{red} , we combine groups of different masses in order to cut down the uncertainties in the f_{red} measurements, which are still fairly large when the galaxy samples are further divided up into r_{grp} bins.

Inspection of Figure 15 shows that at all group-centric radii, the local galaxy density has the strongest influence on the low-mass group galaxies, as is the case in Figure 13. In general, the effect of Σ_5 on f_{red} is similar for galaxies at different group-centric radii. The most massive galaxies subsamples, again, all have high f_{red} (larger than 0.8) for all local densities and group-centric radii. The f_{red} of intermediate-mass galaxies shows a possible weak change with local galaxy density with low significance, but consistent with that measured in Figure 13. For the low-stellar mass group galaxies there is a clear correlation between f_{red} and local galaxy density. This is observed in all group-centric radii, including the core region.

Importantly, note that for the low-mass galaxies, even with local galaxy density controlled, galaxies are on average redder in the center of the group than those in the outskirts. A similar, but weaker, trend is also seen for the intermediate-mass galaxies. This strongly suggests that the location of the (lower-mass) galaxies in their parent group halo has an effect on their evolutionary history, after the effects of local density and stellar mass are controlled. That is, the redder population seen in the center of galaxy groups and clusters is not due entirely to these

galaxies being in a denser region; being in the center of a massive halo also contributes to them turning red.

5. DISCUSSION

5.1. The Uncertainties

Our work is exploited by photo- z , which is known to have less accurate redshift information than spectroscopical measurement. With intricate corrections in weight and background subtraction, we discuss uncertainties in our procedure and possible effects on our results with the aid of mock catalog whose properties are detailed in Croton et al. (2006). We assign photo- z to each mock galaxy such that the overall photo- z dispersion compared to mock redshift is comparable to that in our training set.

5.1.1. w_i

For each galaxy whose photo- z uncertainty is less than $0.6(1+z)$, we assign a weight w_i based on the ratio of the number of all galaxies in the catalog to that in the sample in a given magnitude bin (§2.2). Such w_i is only a function of magnitude, because we find that both blue and red galaxies, roughly separated by $B - R_c = 1.8$, have comparable w_i . The role of w_i is to account for the missing galaxies in a given magnitude bin due to large photo- z errors. In practice, for n galaxies drawn from the sample, the expected total galaxy count is $\sum_{i=0,n} w_i$.

To estimate the effect of w_i , we apply the same w_i computation to the mock catalog with the simulated photo- z . The w_i reaches 2 at $R_c = 22.45$, typical to our observed data. We then compute f_{red} for the mock galaxies at each redshift bin. We find that such f_{red} is smaller by $\sim 10\%$ than that using the known mock redshifts (i.e., no galaxy is removed hence no w_i correction) at each redshift bin. In other words, the w_i correction results in a smaller f_{red} but such effect is uniform over different redshift bins. The zeropoint of the $f_{red} - z$ trend is smaller with w_i applied, but the slope of the trend remains the same.

5.1.2. Missing Groups and Contaminated pFoF Groups

Our group sample is constructed using the pFoF algorithm on the photo- z catalog. No group finding algorithms are known to be perfect, including the pFoF algorithm. We apply the pFoF algorithm to the mock catalog with the simulated photo- z and computed w_i . We test the performance of the algorithm and investigate the roles of missing mock groups and falsely detected and contaminated FoF groups.

First, we find that the pFoF algorithm is able to recover $\geq 80\%$ of the mock groups whose halo mass are $\geq 2 \times 10^{13} M_\odot$ within our redshift range, and the recovery rate is not a strong function of redshift. We compute f_{red} using mock galaxies brighter than $M_{R_c}^* + 1.5$ in each mock group, and investigate the average f_{red} with and without any missing mock groups. Since the recovery rate depends on halo mass, we carry out the comparison in three halo mass bins. We find that for groups with halo mass greater than $10^{13} M_\odot$, approximately the lower limit of our sample, the missing groups have essentially no effect on the average f_{red} , with the value being 1 to 2 % redder for the pFoF recovered groups when compared to the complete mock group catalog. It is only by going down to the halo mass range in halo mass to 1

to $7 \times 10^{12} M_{\odot}$, well below our nominal group mass limit, where we find an effect of about 10%.

Second, we find the fraction of false and contaminated mock pFoF groups is a strong function of redshift and $M_{*,grp}$. We define a contaminated group as a pFoF group with a match from the mock group catalog, but with a significant number of linked galaxies not belonging to the true mock group (see Li & Yee for a precise definition). In principle, in a large sample the effect of groups deemed contaminated on the measurement of f_{red} is expected to be statistically corrected by the background corrections. However, groups contaminated with larger fore- or background galaxies would be more likely to be identified by any FoF algorithm. Thus, we include both false detected groups and contaminated groups in our tests on their effects on the measurements of f_{red} . Hereafter, we will simply refer to these groups as ‘contaminated groups.’ The contaminated groups tend to occur at higher redshift or small $M_{*,grp}$ regime. Since galaxies in contaminated groups are expected to be bluer on average, contaminated pFoF groups makes the $f_{red}-z$ trend slightly steeper in the low $M_{*,grp}$ bin. For the low-mass pFoF mock groups with $M_{*,grp}$ between $10^{11.2}$ and $10^{11.8} M_{\odot}$, the contaminated group fraction is $\sim 20\%$ at $z \lesssim 0.45$, but increases to $\sim 67\%$ at $z \sim 0.5$. Using the mock groups we find f_{red} for the mock pFoF sample at $z \sim 0.25$ to be a factor of ~ 1.07 smaller than the true value, with the discrepancy increasing to ~ 1.23 smaller at $z \sim 0.5$. For the more massive pFoF mock groups, the contaminated fraction is only $\sim 15\%$ at $z \sim 0.5$, resulting in a smaller average f_{red} by $\sim 3\%$. We note that this small effect comes primarily from contaminated groups, rather than false detection groups, as there are negligible number of false massive groups. The contamination fractions at lower redshift are smaller, resulting in negligible effects on f_{red} for the more massive groups.

We note that these pFoF mock groups are selected by $N_{gal} \geq 5$, $N_{gz} \geq 5$ and $M_{*,grp}$, but not by B_{gc} . Based on Fig. 8, the $B_{gc} \geq 125$ cutoff removes 10% of the pFoF groups from the sample. Therefore, if they are further selected by B_{gc} , the above false detection fraction and the difference in the average f_{red} using the mock pFoF groups are expected to be even slightly lower.

As an example, In Figure 10 panel a), the contaminated pFoF groups in our sample make the $f_{red}-z$ trends steeper than the actual slopes. However, based on the above mock tests, we argue that the general declining $f_{red}-z$ trend cannot be simply caused by the increase in contaminated pFoF groups, since the difference in f_{red} between $z \sim 0.25$ and $z \sim 0.5$ is considerably larger than what is expected due to the effect of contaminated groups. To account for the possible systematic effect of false group detection and contaminated groups, we increase the upper uncertainty error bars on f_{red} for the low-mass group bins based on our mock group tests in all Figures involving f_{red} .

5.1.3. Group Centers and Group-centric Radius

In §3.3 we assign a pFoF linked galaxy to be the center of that galaxy group. However, it is not necessary to have a galaxy located at the center. We do so because this allows us to study properties of these ‘central’ galaxies in the future. Another way to define the group center is to take the median position of all the linked galax-

ies weighted by their luminosity and local galaxy surface density. L09 find that such centers for the CNOC1 clusters are about $30''$ from the cD galaxies. For the RCS1 groups in this work, the median separation of these two types of group centers is $\sim 8''$, which is equivalent to 0.04 Mpc at $z=0.3$ or 0.05 Mpc at $z=0.5$.

The R_{200} is another factor which affects the group-centric radius. We compute the R_{200} by extrapolating the $B_{gc}-R_{200}$ relation in Yee & Ellingson (2003). The derived R_{200} for our group sample is $\sim 1.07 \pm 0.24$ Mpc. Therefore, the uncertainty in R_{200} dominates over the role of group center in computing r_{grp} . We note that the $B_{gc}-R_{200}$ relation, which is derived based on the CNOC1 clusters, may not be the same for galaxy groups. However, the relation indeed offers us an efficient way in estimating R_{200} to be within an order of magnitude to the actual values.

The uncertainty in the R_{200} introduces $\Delta \log(M_{*,grp}) \sim 0.1 M_{\odot}$ to the $M_{*,grp}$ in §3.4, and gives a $\Delta f_{red} \sim 0.04$ in the f_{red} computed using group galaxies within $0.5 R_{200}$ of the groups. We believe that our conclusions remain the same even though we have large uncertainties in group-centric radii, because our bin size for $M_{*,grp}$ is large enough to accommodate this extra uncertainty due to R_{200} , and any changes in f_{red} are bigger than 0.04 in general.

5.2. Properties of Group Galaxies

It has been known for decades that galaxy properties correlate with their environment: Galaxies in clusters are dominated by a red population, and field galaxies are characterized by a blue population. The morphology-density relation presented in Dressler (1980) has set the stage for many studies in the following decades to quantify this relationship and to investigate the causes. With the halo model of galaxies and groups, Weinmann et al. (2006) suggest that the morphology-density relation can be expressed in terms of halo mass instead of galaxy number density, because the projected galaxy number in a halo is expected to correlate with the halo mass. A standard picture of the halo model is that some galaxies are embedded in their own individual halos independently, and some reside within a common halo shared with other galaxies in the form of galaxy groups. Once a halo enters within the virial radius of a more massive one, such as when a single-galaxy halo enters a group halo, it is referred to as a satellite halo or sub-halo within the larger halo (or, the parent halo). As the satellite or sub-halo orbits within the more massive one, it may be subjected to all kinds of environmental effects; its mass is reduced and the diffuse outer part can be stripped off by tidal effects and interactions with other substructures. In addition to the mass loss, the gas reservoir of the infalling galaxy will be deprived and eventually lead to a halt in its star formation when the galaxy depletes its cold gas. This is usually referred to as ‘strangulation’ (e.g., Balogh et al. 1999, 2000; van den Bosch et al. 2008; Kawata & Mulchaey 2008; McGee et al. 2009). In this section we discuss the results from our galaxy group sample in the context of the halo model and ‘nature’ versus ‘nurture’ scenarios.

5.2.1. Four Factors that Affect the Group Galaxy Population

We have identified one intrinsic and three global parameters that affect the evolution of the population of group galaxies as measured by the red galaxy fraction, f_{red} . The underlying predominant parameter is the mass of a galaxy’s own halo (measured via the galaxy’s stellar mass). The other three, (1) the mass of the parent group halo into which the galaxy has fallen, (2) the position of the galaxy in the parent halo, and (3) the local galaxy density, produce further effects which evidently accelerate the evolution of the galaxies to their final red color. Here we summarize the observed effects of these four parameters on f_{red} as shown in Figures 10–15.

- The galaxy population as measured by f_{red} is strongly dependent on the galaxy stellar mass; i.e., its own halo mass. The most massive galaxies ($\log(M_*/M_\odot) \geq 11$, or $M_{Rc} \lesssim M_{Rc}^* + 0.6$ for red galaxies) are already mostly red in all group environments by $z \sim 0.5$. The effects of the group environment and the local galaxy density, summarized below, are primarily seen in galaxies with $\log(M_*/M_\odot) < 11$.
- The mass of the parent group halo affects the galaxy population such that the red galaxy fraction is larger for galaxies in more massive groups. This effect is observed after controlling for the stellar mass of the galaxies and it is stronger for lower-mass galaxies.
- The red galaxy fraction has a dependence on the location of galaxies in their parent halo, as parametrized by the group-centric radius, r_{grp} , normalized by R_{200} . The f_{red} for intermediate- and low-mass galaxies increases toward the group center, with the radial gradient being steeper for lower-mass galaxies. For low-mass galaxies, there are also some indications that the f_{red} gradient is steeper for galaxies in more massive groups.
- There is a degeneracy in the two parameters, group-centric radius (r_{grp}) and local galaxy density (Σ_5), that measure the environment of group galaxies. By examining galaxy samples of intermediate and low stellar masses in bins of local galaxy density, we find that: 1) for galaxies in the same local galaxy density bin, there is still a radial gradient in f_{red} ; and 2) conversely, for galaxies at the same group-centric radius, those in higher local galaxy density regions have larger f_{red} . These results indicate that both the position of the galaxy in the parent halo and the local galaxy density around each individual galaxy have an effect on its evolutionary history.

In the following subsections, we discuss in more detail the dependence of f_{red} on these various parameters, and how it fits into the general context of galaxy evolution.

5.2.2. The Dependence on Galaxy Stellar Mass

The *apparent* strength of the dependence of the f_{red} on environmental effects, whether it is the mass of the group halo, the position the galaxies in the halo, or the local galaxy density, is a strong function of the stellar mass of the galaxies. The biggest effects are seen in the lowest mass galaxies; while for the most massive galaxies, those with $\log(M_*/M_\odot) \geq 11$, little discernible environmental effect is found. Furthermore, for these most massive galaxies the f_{red} , which is close to 1, has no apparent dependence on redshift (within our redshift range of $z \lesssim 0.5$) regardless of their group environment. The uniformity of the slope, color zero-point, and dispersion of the stacked red-sequence (Figure 9) for galaxies brighter than M_R^* also points to the conclusion that the most massive galax-

ies in our sample have completed their evolution to a quiescent state by $z \sim 0.5$, suggesting that they mostly formed early and have little or no star formation since $z \sim 1$. Our conclusion that the stellar mass of a galaxy is a more fundamental factor in galaxy evolution echoes the recent spectroscopic results (e.g., Grützbauch et al. 2010; Cucciati et al. 2010; Li et al. 2010; Sobral et al. 2010). This illustrates that our photometric-redshift samples are able to give reliable conclusions while it provides a group sample size much larger than any from spectroscopic surveys at $z \geq 0.15$.

However, that the lowest-mass galaxies appear to be most affected by the group and local density environments does not necessarily mean that these environmental factors produce disproportionately larger effects on low-mass galaxies, or that massive galaxies are immune to them. Rather, it is likely that massive galaxies are equally affected by their environment, but the (secular) galaxy down-sizing evolution effect has already turned most massive galaxies red well before $z \sim 0.5$. And once they are red, the ‘nurturing’ influence can no longer be discerned—whether a galaxy is far away from a parent halo, or in a low galaxy density region, it is already red. The same environmental effects likely have operated on these massive galaxies earlier on, accelerating the process of them turning red, to different degrees for galaxies in different environments. In this interpretation, we should be able to observe similar kinds of dependence of f_{red} on group-centric radius, group halo mass, and local galaxy density for galaxies of larger masses at higher redshifts. By the same token, for intermediate-mass galaxies at lower redshifts, we should expect them to have a smaller apparent dependence of their galaxy colors on group or local galaxy density environments, because many of them would have already turned red by the present epoch.

5.2.3. The Dependence on Group Halo Mass

In the halo model, the infall of a galaxy in a subhalo into the parent group halo is a significant event in the evolution of the stellar component of the galaxy. The larger halo can affect the star formation history of the infalling galaxy via a number of mechanisms that act on a global scale within the parent group, such as strangulation, ram-pressure stripping, and tidal disruption. The dependence of the galaxy population on the mass of their parent group or cluster can provide insights into the efficiency of the various environmental mechanisms that affect star formation history, and their relative importance. There is some evidence from redshift surveys in the local universe that galaxy population properties have a dependence on the mass of the parent group halo, in that galaxies in more massive halos tend to be in a more evolved, or quiescent, state (e.g., Weinmann et al. 2006; Kimm et al. 2009; van den Bosch et al. 2008, L09). At higher redshifts, Iovino et al. (2010), using groups with z up to 1 cataloged from the zCOSMOS survey, found that the galaxy blue fraction is larger for groups of lower richness. We find in our sample a similar dependence in general, and we examine this dependence in more detail as functions of both galaxy stellar mass and group-centric radius.

The dependence of the galaxy population on the parent group halo mass is primarily seen in lower-mass galaxies. Figure 10 also shows that the effect has a redshift de-

pendence. By $z \sim 0.25$, the difference in f_{red} for galaxies in groups of different masses is seen mostly in low-mass galaxies; whereas at $z \geq 0.35$, both intermediate- and low-mass galaxies show a significant dependence of f_{red} on $M_{*,grp}$. Further subdividing the samples by the group-centric radius, we find that the increase in f_{red} for the intermediate- and low-mass galaxies occurs over the range of group-centric radius from the core to outside the virial radius. However, in the core of rich groups galaxies of different masses have a narrower range of f_{red} values, compared to those in poor groups; i.e., the dependence on group-centric radius is stronger for galaxies in rich groups than poor groups. We note that some caution should be used when considering the strength of this effect, in that it is more difficult to define the center of a poor group, which may cause a smearing of the radial dependence. Weinmann et al. (2006) observed a similar dependence of the $f_{red}-r_{grp}$ trend on group mass at $z \sim 0$ using their SDSS group sample, with their lowest mass groups (which are less massive than our low group mass bin) showing almost no dependence of f_{red} on r_{grp} . Over all, this dependence on the group halo mass can be described, to borrow a popular term from galaxy evolution, as some sort of ‘down-sizing’ effect, in that the galaxy population in richer groups appears to be on average in a more advanced stage of their evolution.

Our data demonstrate the additional influence that group environment has on their constituent galaxies, but does the effectiveness of this influence depends on the mass of the parent halo? That is to say, is this apparent ‘group down-sizing’ effect due to the different effectiveness (or prevalence) of the mechanisms that quench the star formation of the accreted member galaxies? While this may be the case, the same effect can also be produced by a simpler explanation: The larger f_{red} in more massive groups can simply be a result of a hierarchical build-up of structures, such that at any given epoch the more massive groups/clusters have been in existence for a longer time than less massive groups. In a scenario where galaxy stellar mass is the primary determinant of the time scale of galaxy evolution, we can consider that group environment is acting as an accelerator for the galaxy to reach its final red quiescent state (e.g., Bolzonella et al. 2010; Balogh et al. 2011). At a fixed redshift, if the time scale for the growth of the group from the accretion of ‘field’ galaxies is longer than that for the truncation of star formation in the galaxies, then the infalling galaxies would turn red faster than the rate of accretion of more field galaxies, creating a situation where groups that have been in existence for a longer time would have a larger fraction of red galaxies. Under this scenario, clusters or groups of a fixed halo mass would expect to have an overall bluer population at higher redshift than those at lower redshift, since, even if their accretion histories are similar, their accretion time scale is compressed (McGee et al. 2009). This situation would naturally produce the Butcher-Oemler effect for a sample of fixed group/cluster mass over a range of redshift.

Observationally it is impossible to trace precisely the evolution of the progenitors of a given group along the redshift axis. Hierarchically, structures grow from smaller systems into larger ones; a rich group at lower redshift is likely to have a smaller mass in the past. In Figure 10, we use fixed $M_{*,grp}$ cutoffs at different redshift

bins without considering such mass evolution. If we could trace the progenitors, i.e., distinguish the ancestors, the apparent Butcher-Oemler effect and the ‘group down-sizing’ effect is expected to be even stronger. For example, a group at $z \sim 0.25$ is expected to have a smaller mass at $z \sim 0.5$, and hence a lower $M_{*,grp}$. Since groups of smaller $M_{*,grp}$ at a fixed redshift have smaller f_{red} , the ‘ $f_{red}-z$ ’ gradient for this group in our example will become even steeper, making the ‘group down-sizing’ effect more significant.

5.2.4. Environmental Influences: The Effect of Local Galaxy Density and Group-Centric Radius

The local galaxy density (Σ_5) and group-centric (or cluster-centric) radius (r_{grp}) are two parameters that are often used to measure the environment of galaxies. In fact there has long been a running discussion in the literature as to which is more fundamental in determining the galaxy population properties of cluster galaxies (e.g., Dressler 1980; Whitmore et al. 1993). While they are correlated with each other, since local galaxy density is higher in the center relative to the outskirts, these two parameters can provide indications of different physical mechanisms. The group-centric radius can be considered as a parameter sensitive to the global environment of the gravitational potential and gas content of the parent group halo. Thus, r_{grp} can be used to gauge the importance of mechanisms such as ram-pressure stripping, strangulation, and global tidal effects from the group dark matter halo mass. On the other hand, local galaxy density measures the more immediate environment, and is more pertinent to mechanisms that are dependent on the existence of neighboring galaxies, such as harassment and galaxy-galaxy interactions and mergers.

In most studies of group or cluster galaxies, where the galaxy samples are usually too small to separate into subsamples of both radial and local-density bins, correlations of galaxy population properties with one or the other parameter become ambiguous. Is the change in the galaxy population as a function of group-centric radius a reflection of the different local galaxy densities at different radii? Or conversely, is the correlation between local galaxy density and galaxy population primarily a result of the position of the galaxies within the larger parent halo in which they reside? These questions can be answered by examining the properties of galaxies at a fixed group-centric radius as a function of local galaxy density, or for galaxies in regions of a specific local galaxy density in different group-centric radii. A similar but more bimodal view is taken by some investigators in which galaxies are simply divided into ‘central’ galaxies and ‘satellite’ galaxies (e.g., van den Bosch et al. 2008).

Figure 15, which plots the f_{red} of group galaxies in different local galaxy density bins as a function of group-centric radius, demonstrates the residual effect of local galaxy density after accounting for the stellar mass of the group galaxies and their positions within their parent groups. Again, the low-mass galaxies show the largest effect (showing up as the separations between points of the same symbols in each panel of Figure 14) due to local galaxy density, where over the factor of about 13 in Σ_5 , f_{red} is changed by roughly 0.2 to 0.5, with the difference being more significant at lower redshift. This change is comparable to the changes seen in f_{red} over the

r_{grp} range from outside R_{200} to the core. Similarly, for the intermediate- and high-mass galaxies, the difference in f_{red} induced by the local galaxy density is also the same order as that seen for these galaxies between $\sim R_{200}$ and the group core: $\Delta f_{red} \leq 0.1$ for the massive galaxies, and about 0.1 to 0.2 for the intermediate galaxies.

In most studies of the effect of local galaxy density on the make-up of galaxy populations, the location of the galaxy within a larger halo is rarely considered (since often, these are “field” samples). Furthermore, the stellar mass effect is clearly dominant over that of local galaxy density. Thus, if neither of these are controlled, the local galaxy density correlation could become misleadingly strong. There are several investigations of the effect of local galaxy densities for field galaxies in which the mass or luminosity of the galaxies is taken into consideration. Using the same RCS1 photometric redshift catalog as a field sample between z of 0.2 and 0.6, Yee et al. (2005) found almost no dependence of f_{red} on local galaxy density at $z \geq 0.5$, and a weak dependence at $z \sim 0.3$, whereas Balogh et al. (2004) found using the SDSS at $z \sim 0$ a strong local galaxy density dependence of f_{red} for galaxies of all luminosities. More recently, Baldry et al. (2006) and Peng (2010), using SDSS data, show that most of the dependence of f_{red} on environment primarily occurs for galaxies with $\log(M_*/M_\odot) \leq 10.7$.

Our results, after controlling for group environment, show a similar trend to that found by Baldry et al. (2006) for SDSS galaxies. Because none of the three parameters, M_* , Σ_5 , and f_{red} , are computed identically in different studies, we can only compare the dependence of f_{red} from the two studies approximately. Our three density bins center cover a range of approximately 1.1 dex in Σ_5 , each with a half bin width of approximately 0.27 dex. It is reasonable to match the local galaxy density parameters, (Σ_5 in this paper, and Σ in Baldry et al. (2006)), by assuming that the high ends of the density measurements are similar. Hence, the high- and low-density bins in our work correspond to approximately $\log \Sigma \sim 0.8$, and -0.3 in Baldry et al. From their Figure 11, and averaged over similar bins of galaxy stellar mass, the change in f_{red} , Δf_{red} , between local density bins equivalent to our low and high bins are ~ 0.1 , 0.2 , and 0.3 for stellar masses of $\log(M_*/M_\odot) > 11.0$, $10.6 \leq \log(M_*/M_\odot) < 11.0$, and $10.2 \leq \log(M_*/M_\odot) < 10.6$, respectively. These relative changes in f_{red} for different local galaxy densities from the SDSS field galaxy sample are consistent with what we find for the group galaxy sample at $z \sim 0.25$, with $\Delta f_{red} \sim 0.1$, 0.25 , and 0.4 for the three stellar mass bins, respectively.

We also find that the relative effect of local density on f_{red} is roughly constant as a function of group-centric radius and the mass of the parent group halo. This, along with the general agreement with the effect for field galaxies, suggests that we can separate the influence between local galaxy density and the global effects of the group environment. In the context of the debate of whether galaxy population is correlated primarily with local galaxy density or cluster/group-centric radius, our results indicate that both parameters are important.

5.2.5. Galaxy Groups as the ‘Nurturing’ Influence

In early discussions of Dressler’s work on the ‘morphology-density’ relation (Dressler 1980), along with

the discovery of the Butcher-Oemler effect (Butcher & Oemler, 1978), attempts to interpret the results along the lines of the idea of ‘nature’ versus ‘nurture’ have often been used, though not much has been resolved (e.g., Poggianti et al. 1999; Cooper et al. 2007; Mateus et al. 2007; Tasca et al. 2009). From the perspective of the halo model, we can invoke this classic framework in the following way. The strong dependence of a galaxy’s star formation history on its own halo mass can be attributed to ‘nature;’ while how it interacts with its immediate neighboring subhalos and how it is being influenced by the larger group halo into which it has been accreted can be thought of as the ‘nurturing’ processes. (There can be some debate as to whether the local galaxy density can be considered as part of the ‘nature’ process; it could be that a galaxy is more likely to be massive because it was formed in a high-density region.) The dependence of the red galaxy fraction on the stellar mass of galaxies can be seen as a manifestation of the currently accepted down-sizing star formation paradigm, and considered as the underlying secular evolution of a galaxy.

After controlling for both galaxy stellar mass and local galaxy density, our data clearly show a residual dependence of the red galaxy fraction on the group environment, especially for lower-mass galaxies. Group galaxies show a f_{red} gradient with the group-centric radius, in that galaxies in the center are redder on average than those further out. Furthermore, this effect is larger in more massive groups. This gradient is not entirely due to the fact that local galaxy density is higher in the core of a group, since it is still seen using galaxy samples in fixed bins of Σ_5 . The change in f_{red} going from outside R_{200} to the core is comparable to or larger than the changes seen in f_{red} due to a change of local density of a factor of ~ 13 times. This suggests that the efficiency in truncating star formation from physical processes arising from close neighbors is of the same order as that due to the processes operating in the larger halo into which the galaxy has been subsumed.

Physical processes that are related to neighboring galaxies include galaxy mergers and harassment, producing strong tidal effects on the galaxy. We can consider the local galaxy density effect to be part of the secular evolution, on top, or part, of the down-sizing effect; i.e., these effects occur independently of whether a galaxy with certain local galaxy density is sitting in the field, or in the outskirts, or within the virialized region of a larger group. However, the much more massive group halo may produce ram-pressure stripping due to intra-group gas, or a strangulation effect from the removal of the outer gaseous halo of the infalling galaxy. Such processes can serve as additional mechanisms in driving the galaxy evolution towards the red-and-dead state. The net effect is an acceleration of the truncation of star formation as the galaxy settles into the parent halo, turning it red earlier than field galaxies of similar stellar masses which are not affected by a group halo.

In the current literature, a number of investigators have separated the effect of stellar mass and environment. For example, Peng (2010) modeled the evolution of galaxy population using the concept of mutually independent “mass-quenching” and “environment-quenching” efficiencies. McGee et al. (2009) used the idea of “fraction of environmentally affected galaxies”,

based on accretion history of galaxy groups and clusters from n-body simulations, to model the evolution of cluster galaxy populations. We note that these two studies effectively focused on two different environmental parameters – Peng et al. on local galaxy density, and McGee et al. on group environment. In the analysis of our large sample of group galaxies, we find that we can in fact separate the environmental effect into a local galaxy density effect and a more global large scale structure effect due to the presence of a larger group mass halo into which the subhalo has been accreted. These two types of effects likely invoke different mechanisms that lead to environmental quenching of star formation in the accreted galaxies, and both need to be accounted for explicitly in modeling galaxy evolution.

In a picture where the the dependence of star formation rate on stellar mass is considered as the long term secular trend in the evolution of a galaxy, the local galaxy density environment can accelerate the quenching rate of star formation, but over different time scales, depending on the process. For example, galaxy mergers can act as a one-time-only process that happens stochastically and quickly change the nature of the galaxy; whereas galaxy harassment can be a more gentle process acting over a longer time scale. The other major environmental event is the accretion of a galaxy into a larger halo, which will further act as an accelerator in the evolution of the galaxy. This would be a short-time-scale, one-time-only event as the galaxy approaches the group virial radius, where its star formation is quenched due to processes that are associated with the large gravitational potential of the massive group halo. A detailed study of dependence of star formation history of galaxies on these parameters based the mass of the galaxy, and the local and global environments, will ultimately lead us to a better understanding of galaxy evolution.

6. SUMMARY

Using 905 galaxy groups identified by the pFoF algorithm in the RCS1 photometric-redshift sample and covering a group total halo mass range of $\sim 10^{13.2} M_{\odot}$ to $\sim 10^{14.5} M_{\odot}$, we study the group galaxy population over the redshift range $0.15 \leq z < 0.52$. We examine the color-magnitude diagram of group galaxies as a function of redshift and group richness, and consider the effects of four parameters on the red galaxy fraction f_{red} and its evolution: the galaxy stellar mass M_* , the total group stellar mass $M_{*,grp}$ (as a proxy for the group halo mass), the group-centric radius r_{grp} , and local galaxy density Σ_5 .

We find the bright end (brighter than M_{Rc}^*) of the red-sequences in the CMD for stacked groups in redshift and group halo mass bins to be remarkably uniform, with their zero point, slope, and dispersion consistent with those found for clusters. Thus, the bright end of the red sequence is already in place, and likely formed at $z \geq 2$, even for those in groups approximately an order of magnitude less massive than clusters.

Most of the evolutionary effects are seen in galaxies of lower stellar mass (strongest for $M_* \lesssim 10^{10.6} M_{\odot}$). We find that groups at lower redshifts possess larger f_{red} than those at higher redshifts, exhibiting a group Butcher-Oemler effect. Examining the dependence of f_{red} in more detail, we find:

1. There is a strong dependence of f_{red} on galaxy stellar mass. More massive galaxies have larger f_{red} , and the group Butcher-Oemler effect is seen within our redshift range only for galaxies with $M_* \lesssim 10^{11} M_{\odot}$.
2. The strength of the dependence of f_{red} on the environmental parameters is also a strong function of the galaxy stellar mass. Galaxies with $M_* \gtrsim 10^{11} M_{\odot}$ are almost all red, independent of their local galaxy density, group-centric radius, and group halo mass. In the items that follow, the results apply primarily for galaxies with $M_* \lesssim 10^{11} M_{\odot}$.
3. We find a dependence of f_{red} on $M_{*,grp}$, in that galaxies in more massive groups have a larger f_{red} . This is seen after the group galaxies are separated into r_{grp} or Σ_5 bins. This effect is strongest for the lowest mass galaxies. The group Butcher-Oemler effect appears to be stronger in lower-mass groups over this redshift range; i.e., the change of f_{red} from the $z \sim 0.5$ to the $z \sim 0.2$ bin is larger for lower-mass groups. This difference is probably at least in part due to low-mass groups starting from a lower f_{red} at $z \sim 0.5$.
4. There is a dependence of f_{red} on group-centric radius, which is stronger for lower-mass galaxies. This dependence still exists after controlling for local galaxy density, but is somewhat reduced. The $f_{red}-r_{grp}$ trend is weak for the low-mass groups, especially in the two higher-redshift bins. While this difference may be real, part of it may be contributed by the larger uncertainty in determining the group center and/or larger contamination for the lower-mass groups.
5. While group-centric radius and local galaxy density are correlated, nevertheless, at a fixed r_{grp} , there is still a significant dependence of f_{red} on Σ_5 . The typical change in f_{red} over a factor of about 13 in Σ_5 is similar to that found in the lower-redshift SDSS ‘‘field’’-galaxy sample, i.e., without controlling whether the galaxies are in clusters or groups. This change is also similar in magnitude to the change in f_{red} seen in galaxies from outside the virial radius to the group core. The dependence on Σ_5 is also larger for lower-mass galaxies. This indicates that group environment has a residual effect over that of local galaxy environment (or vice versa), and the two must be considered at the same time.

A general picture for galaxy evolution, and in particular for galaxies in groups and clusters, emerges from these correlations and other work in the literature at different redshifts. Within the four parameters that we have examined, in a ‘nature versus nurture’ scenario, we can consider the galaxy stellar mass as the predominant determinant of the evolutionary history of a galaxy. This would be the effect that produces the commonly accepted ‘down-sizing’ of galaxy evolution. The environmental influence on this secular trend, which accelerates the galaxy

to its final red state, can be considered as the ‘nurturing’ part of the galaxy’s history. There is some room left as to the debate of whether local galaxy density is part of the intrinsic character of the galaxy, in that galaxies born in a high density region may likely be preferentially more massive. However, local galaxy density, as an influence on galaxy evolution may occur with different time scales and stochastically; e.g., galaxy harassment may be continuous, while galaxy mergers are a significantly shorter time scale event that occur more rarely. On the other hand, the effect of a galaxy falling into and being subsumed by a more massive halo is most likely a one-time-only effect that quenches the star formation in the galaxy over a relatively short time scale. These environmental events all have lasting effects on a given galaxy and the build-up of galaxy groups and clusters. To truly understand galaxy evolution, we need to have samples that cover a wide redshift range and are sufficiently large for us to clearly separate the effects of these parameters. This will then allow us to test the predictions, or inform the construction, of a variety of models and simulations.

The recently completed RCS-2 (Gilbank et al. 2011) with a data set that will provide a similar sample of galaxy groups ~ 25 times larger than the current sample will allow us to make great strides toward this goal.

The data in this paper are based on observations obtained at the Canada-France-Hawaii Telescope (CFHT) which is operated by the National Research Council of Canada, the Institut National des Sciences de l’Univers of the Centre National de la Recherche Scientifique of France, and the University of Hawaii. I.H.L. acknowledges financial support from Swinburne University of Technology and the University of Toronto Fellowship. The RCS and the research of H.K.C.Y. are supported by grants from the Natural Science and Engineering Research Council of Canada and the Canada Research Chair program. H.K.C.Y. also wishes to thank the Academia Sinica Institute of Astronomy and Astrophysics for their hospitality during the latter stage of the writing of the paper.

REFERENCES

- Andreon, S., Quintana, H., Tajer, M., Galaz, G., & Surdej, J. 2006, *MNRAS*, 365, 915
- Baldry, I. K., Balogh, M. L., Bower, R. G., Glazebrook, K., Nichol, R. C., Bamford, S. P., & Budavari, T. 2006, *MNRAS*, 373, 469
- Balogh, M. L., Morris, S. L., Yee, H. K. C., Carlberg, R. G., & Ellingson, E. 1999, *ApJ*, 527, 54
- Balogh, M. L., Navarro, J. F., & Morris, S. L. 2000, *ApJ*, 540, 113
- Balogh et al., M. 2004, *MNRAS*, 348, 1355
- Balogh et al., M. L. 2007, *MNRAS*, 374, 1169
- . 2009, *MNRAS*, 398, 754
- Balogh, M. L., McGee, S. L., Wilman, D. J., Finoguenov, A., Parker, L. C., Connolly, J. L., Mulchaey, J. S., Bower, R. G., Tanaka, M., & Giodini, S. 2011, *MNRAS*, 412, 2303
- Barkhouse, W. A., Yee, H. K. C., & López-Cruz, O. 2007, *ApJ*, 671, 1471
- Bartelmann et al., M. 1996, *A&A*, 313, 697
- Bell, E. F., McIntosh, D. H., Katz, N., & Weinberg, M. D. 2003, *ApJS*, 149, 289
- Berlind et al., A. A. 2006, *ApJS*, 167, 1
- Bolzonella et al., M. 2010, *A&A*, 524, A76+
- Botzler, C. S., Snigula, J., Bender, R., & Hopp, U. 2004, *MNRAS*, 349, 425
- Bower, R. G., Lucey, J. R., & Ellis, R. S. 1992, *MNRAS*, 254, 601
- Brough, S., Forbes, D. A., Kilborn, V. A., & Couch, W. 2006, *MNRAS*, 370, 1223
- Butcher, H. & Oemler, Jr., A. 1984, *ApJ*, 285, 426
- Carlberg, R. G., Yee, H. K. C., Morris, S. L., Lin, H., Hall, P. B., Patton, D. R., Sawicki, M., & Shepherd, C. W. 2001, *ApJ*, 563, 736
- Cassata et al., P. 2007, *ApJS*, 172, 270
- Cattaneo, A., Dekel, A., Faber, S. M., & Guiderdoni, B. 2008, *MNRAS*, 389, 567
- Cooper et al., M. C. 2006, *MNRAS*, 370, 198
- . 2007, *MNRAS*, 376, 1445
- . 2008, *MNRAS*, 383, 1058
- Cowie, L. L., Songaila, A., & Barger, A. J. 1999, *AJ*, 118, 603
- Cowie, L. L., Songaila, A., Hu, E. M., & Cohen, J. G. 1996, *AJ*, 112, 839
- Croton et al., D. J. 2006, *MNRAS*, 365, 11
- Cucciati et al., O. 2010, *A&A*, 524, A2+
- D’Agostini, G. 2004, *ArXiv Physics e-prints*
- Domínguez, M. J., Zandivarez, A. A., Martínez, H. J., Merchán, M. E., Muriel, H., & Lambas, D. G. 2002, *MNRAS*, 335, 825
- Dressler, A. 1980, *ApJ*, 236, 351
- Eke et al., V. R. 2004, *MNRAS*, 348, 866
- Ellingson, E., Lin, H., Yee, H. K. C., & Carlberg, R. G. 2001, *ApJ*, 547, 609
- Ellis, R. S., Smail, I., Dressler, A., Couch, W. J., Oemler, Jr., A., Butcher, H., & Sharples, R. M. 1997, *ApJ*, 483, 582
- Font et al., A. S. 2008, *MNRAS*, 1000
- Fukugita, M., Hogan, C. J., & Peebles, P. J. E. 1998, *ApJ*, 503, 518
- Geller, M. J. & Huchra, J. P. 1983, *ApJS*, 52, 61
- Gerke et al., B. F. 2005, *ApJ*, 625, 6
- . 2007, *MNRAS*, 376, 1425
- Ghigna, S., Moore, B., Governato, F., Lake, G., Quinn, T., & Stadel, J. 1998, *MNRAS*, 300, 146
- Giavalisco et al., M. 2004, *ApJ*, 600, L93
- Gilbank, D. G., Gladders, M. D., Yee, H. K. C., & Hsieh, B. C. 2011, *AJ*, 141, 94
- Gladders, M. D., Lopez-Cruz, O., Yee, H. K. C., & Kodama, T. 1998, *ApJ*, 501, 571
- Gladders, M. D. & Yee, H. K. C. 2005, *ApJS*, 157, 1
- Gladders, M. D., Yee, H. K. C., Majumdar, S., Barrientos, L. F., Hoekstra, H., Hall, P. B., & Infante, L. 2007, *ApJ*, 655, 128
- Gómez et al., P. L. 2003, *ApJ*, 584, 210
- Goto et al., T. 2003, *PASJ*, 55, 757
- Grützbauch, R., Conselice, C. J., Varela, J., Bundy, K., Cooper, M. C., Skibba, R., & Willmer, C. N. A. 2010, *MNRAS*, 1856
- Hashimoto, Y. & Oemler, A. J. 2000, *ApJ*, 530, 652
- Hildebrandt, H., Arnouts, S., Capak, P., Moustakas, L. A., Wolf, C., Abdalla, F. B., Assef, R. J., Banerji, M., Benítez, N., Brammer, G. B., Budavári, T., Carliles, S., Coe, D., Dahlen, T., Feldmann, R., Gerdes, D., Gillis, B., Ilbert, O., Kotulla, R., Lahav, O., Li, I. H., Miralles, J., Purger, N., Schmidt, S., & Singal, J. 2010, *A&A*, 523, A31+
- Hsieh, B. C., Yee, H. K. C., Lin, H., & Gladders, M. D. 2005, *ApJS*, 158, 161
- Iovino et al., A. 2010, *A&A*, 509, A40+
- Kawata, D. & Mulchaey, J. S. 2008, *ApJ*, 672, L103
- Kimm et al., T. 2009, *MNRAS*, 394, 1131
- Knobel et al., C. 2009, *ApJ*, 697, 1842
- Kodama, T. & Arimoto, N. 1997, *A&A*, 320, 41
- Kodama, T., Smail, I., Nakata, F., Okamura, S., & Bower, R. G. 2001, *ApJ*, 562, L9
- Lewis et al., I. 2002, *MNRAS*, 334, 673
- Li, I. H., Glazebrook, K., Gilbank, D., Balogh, M., Bower, R., Baldry, I., Davies, G., Hau, G., & McCarthy, P. 2010, *MNRAS*, 1805
- Li, I. H. & Yee, H. K. C. 2008, *AJ*, 135, 809
- Li, I. H., Yee, H. K. C., & Ellingson, E. 2009, *ApJ*, 698, 83
- Lilly, S. J., Le Fevre, O., Hammer, F., & Crampton, D. 1996, *ApJ*, 460, L1+
- Longair, M. S. & Seldner, M. 1979, *MNRAS*, 189, 433
- Madau, P., Ferguson, H. C., Dickinson, M. E., Giavalisco, M., Steidel, C. C., & Fruchter, A. 1996, *MNRAS*, 283, 1388

- Martínez, H. J. & Muriel, H. 2006, *MNRAS*, 370, 1003
- Mateus, A., Sodré, L., Cid Fernandes, R., & Stasińska, G. 2007, *MNRAS*, 374, 1457
- McGee, S. L., Balogh, M. L., Bower, R. G., Font, A. S., & McCarthy, I. G. 2009, *MNRAS*, 400, 937
- Mulchaey, J. S. & Zabludoff, A. I. 1998, *ApJ*, 496, 73
- Navarro, J. F., Frenk, C. S., & White, S. D. M. 1996, *ApJ*, 462, 563
- Oemler, A. J. 1974, *ApJ*, 194, 1
- Peng, Y. e. a. 2010, *ApJ*, 721, 193
- Poggianti, B. M. 1997, *A&AS*, 122, 399
- Poggianti, B. M., Smail, I., Dressler, A., Couch, W. J., Barger, A. J., Butcher, H., Ellis, R. S., & Oemler, Jr., A. 1999, *ApJ*, 518, 576
- Poggianti et al., B. M. 2006, *ApJ*, 642, 188
- Popesso, P., Biviano, A., Böhringer, H., & Romaniello, M. 2007, *A&A*, 464, 451
- Quadri et al., R. 2007, *ApJ*, 654, 138
- Robotham, A., Wallace, C., Phillipps, S., & De Propriis, R. 2006, *ApJ*, 652, 1077
- Sandage, A. & Visvanathan, N. 1978, *ApJ*, 225, 742
- Seymour et al., N. 2008, *MNRAS*, 386, 1695
- Sobral, D., Best, P. N., Smail, I., Geach, J. E., Cirasuolo, M., Garn, T., & Dalton, G. B. 2010, *MNRAS*, 1657
- Söchting, I. K., Huber, M. E., Clowes, R. G., & Howell, S. B. 2006, *MNRAS*, 369, 1334
- Springel et al., V. 2005, *Nature*, 435, 629
- Stanford, S. A., Eisenhardt, P. R., & Dickinson, M. 1998, *ApJ*, 492, 461
- Tago, E., Einasto, J., Saar, E., Tempel, E., Einasto, M., Vennik, J., & Müller, V. 2008, *A&A*, 479, 927
- Tanaka, M., Goto, T., Okamura, S., Shimasaku, K., & Brinkmann, J. 2004, *AJ*, 128, 2677
- Tasca et al., L. A. M. 2009, *A&A*, 503, 379
- van den Bosch, F. C., Aquino, D., Yang, X., Mo, H. J., Pasquali, A., McIntosh, D. H., Weinmann, S. M., & Kang, X. 2008, *MNRAS*, 387, 79
- Verdugo, M., Ziegler, B. L., & Gerken, B. 2008, *A&A*, 486, 9
- Vogt et al., N. P. 2005, *ApJS*, 159, 41
- Weinmann, S. M., van den Bosch, F. C., Yang, X., & Mo, H. J. 2006, *MNRAS*, 366, 2
- Whitmore, B. C., Gilmore, D. M., & Jones, C. 1993, *ApJ*, 407, 489
- Wilman, D. J., Balogh, M. L., Bower, R. G., Mulchaey, J. S., Oemler, A., Carlberg, R. G., Morris, S. L., & Whitaker, R. J. 2005, *MNRAS*, 358, 71
- Wilman, D. J., Pierini, D., Tyler, K., McGee, S. L., Oemler, Jr., A., Morris, S. L., Balogh, M. L., Bower, R. G., & Mulchaey, J. S. 2008, *ApJ*, 680, 1009
- Wilman et al., D. J. 2005, *MNRAS*, 358, 88
- Worthey, G. 1994, *ApJS*, 95, 107
- Yee, H. K. C. & Ellingson, E. 2003, *ApJ*, 585, 215
- Yee, H. K. C., Hsieh, B. C., Lin, H., & Gladders, M. D. 2005, *ApJ*, 629, L77
- Yee, H. K. C. & López-Cruz, O. 1999, *AJ*, 117, 1985
- Yee et al., H. K. C. 2000, *ApJS*, 129, 475